# CHARACTERIZATION OF ASYMMETRIC FABRY PEROT REFLECTION MODULATORS AT 1.55 MICRONS USING A TUNABLE CW ERBIUM FIBER LASER

A Thesis

Submitted to the Faculty

of

Purdue University

by

Daniel E. Leaird

In Partial Fulfillment of the

Requirements for the Degree

of

Master of Science

December 1996

This thesis is dedicated to my family who has been a constant source of support and encouragement through life's difficult decisions. Specifically, I would like to dedicate this work to my wife, Jennifer, who has put up with me through nine years of marriage (so far) and my children Ian and Maclaine.

# ACKNOWLEDGMENTS

Special thanks to Andrew Weiner for the many years of supervision, mentoring, and friendship. Without his support, none of this would have been possible.

I would like to thank Valeria Da Silva of Corning for interesting discussions and guidance, Paul Wysocki of Lucent Technologies for the optical fiber that was used in the final laser system described herein, Ben Yoo of Bellcore for the loan of the modulator array, and Claude Harrington of Purdue University for guidance in the design and construction of the probe tips.

# TABLE OF CONTENTS

# LIST OF FIGURES

# ABSTRCT

Leaird, Daniel E. M.S., Purdue University, December 1996. Characterization of Asymmetric Fabry Perot Reflection Modulators at 1.55 Microns Using a Tunable CW Erbium Fiber Laser. Major Professor: Andrew M. Weiner.

Future optical communications networks will require high speed modulators to act as the interface between the electronic and optical domains. While single modulators are certainly of interest, arrays of modulators may be of greater interest particularly when considering the ability to multiplex multiple electronic signals onto a single optical stream by way of optical pulse shaping technology.

High speed InP based modulators that had been previously reported to give a 15 dB on-off ratio at 20 GHz were investigated in an array configuration of 18 modulators. As an initial step into determining the feasibility of employing these modulator arrays, utilizing an InP based asymmetric Fabry-Perot structure in a reflection geometry, into an optical pulse shaping apparatus, a CW characterization source was constructed to determine the electrical bias dependent reflectivity versus wavelength in the 1.55 μm band. Various measurement topologies were also investigated in order to determine which geometry could yield the most repeatable results. Finally, modeling of the device structure was completed in order to investigate the source of measured experimental results, and to provide insight into the repeatability of device fabrication. The experimental and theoretical results afford a level of understanding of the characteristics of these devices and some of the steps necessary in order to successfully employ them as arrays in an optical pulse shaper.

# 1. INTRODUCTION

Future optical communication systems may require the ability to modulate electronic data onto an optical data stream at very high rates. Due to the limitations of electronic processing, it is unlikely to believe that a single electronic data stream will be placed onto the optical stream when the highest data rates are utilized. In order to increase the system throughput some degree of parallelism seems inevitable. Depending on the communication system architecture and the cost/availability of system components, various schemes could be imagined to magnify the system throughput.

Multiple electronic data streams could be individually modulated onto an optical stream, either by amplitude modulating a laser diode or employing a fast modulator independent from the laser, and then multiplexed together in order to form a high data rate optical stream. While individual high speed modulators are certainly of interest to this application, modulator arrays may be able to increase the communication system performance using a single high speed laser at a lower cost than multiple lasers and modulators through the use of optical pulse shaping technology. The work of this thesis is centered around an effort to exploit high speed modulator technology in the all important 1.55 μm communications band.

The device array to be investigated is an InP based electro-absorption modulator configured in an asymmetric Fabry-Perot cavity. The Fabry-Perot structure permits high contrast between the on state and the off state of the modulator by shifting the absorption within the cavity with applied bias so that the reflected optical field adds destructively to the incident field. If a fully operational array of asymmetric Fabry-Perot modulators were realized, at minimum, optical pulse shaping [1-2] demonstrations at communications rates would be possible - something that to date has not been accomplished. With continued effort, demonstration of a novel optical communication system testbed may even be

possible. However, before any pulse shaping experiments can be initiated, the individual devices that constitute an array must be investigated.

In order to effectively utilize any novel device, its operational parameters must be carefully characterized in order to determine performance attributes and limits. This characterization may under some conditions be carried out within the final intended system; however, this characterization mode can frequently prove to be very difficult. In order to de-couple the system from the novel component, a characterization system is frequently constructed. This document details the construction of a characterization system intended to measure the spectrally dependent reflection of light from a small active area device or material in the vicinity of the minimum loss band of optical communication fibers.

A continuous wave (CW) tunable erbium fiber laser was constructed with high output power and reasonably broad tuning range to serve as the optical source for the characterization system. Various components such as gain medium and output coupler were studied in order to determine the optimum operating laser for this characterization system.

The completed tunable laser was used to investigate system geometries for measuring the spectrally dependent reflection of asymmetric Fabry-Perot modulators. After discovering a host of difficulties with a simple 'vertical' geometry, a video microscope/probe station was constructed in the 'horizontal' geometry that allowed optical access with a tunable infrared laser beam, electrical access for modulator bias, and visual access via a closed-circuit camera/monitor. Using the completed electro-optical measurement system, the reflection characteristics of individual modulators composing the array were measured. Unfortunately, the modulation depth of this sample, provided by an external collaborator, was significantly lower than that shown in previously published results.

In order to explore the source of the decreased modulation depth, theoretical calculations were undertaken. The model matched the previously published results very closely, and, with minor modifications, could be used to explain the discrepancy between the measurements made during the course of this work and the earlier work.

# 2. CW TUNABLE ERBIUM FIBER LASER

## 2.1 Introduction

It is true that the major topic of this thesis is the characterization of an asymmetric Fabry-Perot reflection modulator; however, before any characterization could take place, an optical characterization source had to be created. Coupled with the desired design space for this source - high power, large tuning range - was the need to keep the financial cost minimized. This necessity initially required the use of erbium-doped optical fibers that had been previously donated to our group as the laser gain medium even though these fibers may not have been what one would select for a high power CW fiber laser.

Several different erbium doped fibers were explored to determine which would provide the highest output power while maximizing the available tuning range. In order to start this exploration, long lengths of erbium fiber were inserted into a simple linear cavity. As much pump power as possible was coupled into the cavity while the laser action, if any, was monitored on an optical spectrum analyzer. The erbium fiber length was reduced systematically in order to determine over what range of fiber lengths laser action was possible and with what output power. The process of selecting the optimum gain medium, the test laser cavity design, final cavity design, and final optical characteristics are detailed in the following sections.

## 2.2 Gain Medium Measurements

The very first experiments conducted in any of the work described in this thesis involved an attempt to identify the properties of erbium doped optical fiber previously donated to our group. Characterization was performed in a very simple manner. The optical pump, CW light at 980 nm from a commercial titanium-sapphire (Ti:S) laser, was coupled into one end of a piece of optical fiber doped with the rare earth element erbium. The other end was connected to an optical spectrum analyzer (OSA) utilizing a bare-fiber

adapter. The optical spectrum of the emission of a piece of erbium fiber was monitored as a function of fiber length and optical pump power. These spectra were then repeated for fibers of different doping levels.

The erbium fiber has the property that it absorbs the 980 nm light and emits, or fluoresces, in the 1.4 μm to 1.6 μm wavelength range. The shape, position, and width of the optical spectrum of this fluorescence is determined by the amount of pump light coupled into the fiber, number of erbium atoms per unit volume in the optical fiber, fiber length, and any loss mechanisms present. The character of the ASE from fibers of different doping levels and lengths was monitored on the OSA. Initially, optical spectra were recorded on paper by means of screen-dumps of the OSA display. Later, a data capture program was written that allowed these spectra to be collected and recorded on a laboratory computer; thus, simplifying the archiving of data.

The general characteristics of the gain spectra of erbium doped fiber are well known, and have been widely reported. A gain peak at 1.532 μm and span of approximately 1.528 μm to 1.570 μm is what one would expect to see from erbium doped optical fiber based on an abundance of information in the public domain. Due to preconceived notions of what the ASE spectrum of the donated fibers should look like, and based on information from commercial sources, a large amount of time was spent investigating unusual ASE characteristics of the fibers. Figure 2.1 shows the ASE spectrum of a 5 m length of fiber known as ErCaAl081790-082090. This spectrum shows two emission peaks - one at about 1.4 μm, and one at 1.6 μm with nothing in the 1.5 μm band. Clearly, this does not conform to what one would consider to be a 'normal' erbium doped fiber. A literature search using the THOR system at Purdue gave the impression that this sort of character was unknown to the scientific community. Certainly 'standard' erbium fibers had been widely investigated, but the fibers we had were very non-standard in that they were designed for short pulse laser operation with much higher doping levels than is used in fibers designed for amplifiers configurations. This rather loose justification, coupled with the inadequate literature search conspired to temporarily redirect this work away from the modulator characterization toward the development of a novel laser source that might permit tuning out to 1.6 μm using erbium doped optical fiber as the gain

medium. Due to low output powers in the long wavelength regions, for reasons to be discussed later, further effort was not expended on developing these laser systems.

### 2.3 Cavity Selection/Design

Prior to making any decision about the cavity design to be employed in the final laser system, a fairly exhaustive literature search was undertaken in order to determine the design trade-offs of various cavity designs. The performance criteria considered were large continuous tuning range and high output power levels. The various schemes reviewed, while all somewhat different as would be expected, fell into two categories, either electronically tunable laser systems [3-9], or mechanically tunable systems [10-12].

The electronically tunable systems, while certainly attractive as far as measurement system automation is concerned, tended to suffer from relatively small tuning ranges as compared to the mechanically tuned systems. The output powers in both types of systems tended to vary substantially; however, since the designs reviewed were constructed near the beginning of the rush of interest in erbium doped fiber as a gain medium, the output power variance can most probably be attributed to differences in the gain medium rather than inherent problems with the tuning element. Since the mechanically tuned systems tended to have larger tuning ranges than the electronically tuned systems, the mechanical tuning style was selected as the cavity configuration of choice for this laser system.

Figure 2.2 shows a simple schematic of the design selected. Modeled after [10], it is a simple linear cavity with a wavelength selective element used as one end mirror and the output coupler as the other end mirror. The wavelength selective element, a diffraction grating, is mounted in the Littrow configuration so that, as a function of rotation angle, different frequency components (or wavelengths) are reflected back to the gain media thus enhancing the gain at that particular wavelength while introducing loss at all other wavelengths. The output coupler reflectivity could be made as low as 4% by flat cleaving the fiber end face and using that end face as the output coupler, or as high as 99% by butt coupling the fiber end face to a high reflector. The diffraction grating could also be made into a general high reflector for all wavelengths by simply rotating it to normal incidence and using the specular reflection. With this configuration, it was possible to determine the range of wavelengths laser action was possible as a function of

gain medium absorption (by way of doping concentration and fiber length) by varying the pump power and mirror reflectivity's.

## 2.4 Investigations of Tuning Range & Output Power vs. Output Coupling and Doping Level

For all fibers that were investigated, the starting point was always to insert the fiber into the cavity by fusion splicing it to the wavelength-division multiplexer (WDM) coupler; then, rotate the diffraction grating to normal incidence. Pump light was then coupled into the cavity and the system output was monitored on the OSA. The reason for rotating the diffraction grating to normal incidence is that in this configuration the cavity loss was minimized for all wavelengths making it possible to determine if lasing action was even possible within the available amount of pump light for the length of erbium doped fiber being investigated. If lasing action was not seen (at the gain peak of the ASE) for even the highest possible pump powers, the fiber length was reduced until it was possible to make the system lase. The output coupler reflectivity could also be varied, to a limited extent by moving from a flat cleave on the fiber end face (giving a 4% reflector) to butt coupling to a high reflectivity output coupler - typically in the 80 - 90% reflectivity range.

All of the earliest fibers that had been donated to our lab had been designed as short pulse laser fibers. This means that the erbium doping level was higher in these fibers than is seen in typical fibers designed for optical amplifier configurations. These high doping levels allow short gain medium lengths so as to keep the dispersion of the cavity low; however, they also tend to enhance other loss mechanisms - most notably excited state absorption[13]. In using the highly doped fibers in this CW fiber laser, several trends were evident. Tuning to longer wavelengths was possible for longer fiber lengths; however, the lasing threshold increased as well thus limiting the output power for a fixed maximum pump input. A typical fiber length that would give a reasonable tuning range (in excess of 50 nm) was 50 cm for several hundred milliwatts of pump light coupled into the fiber. With the fiber this short, the output power would be on the order of 100 μW.

Concerns over the low output power available from these fibers lead to inquires with experts in fiber laser systems at Corning and Bell Labs. It was in these discussions that excited state absorption was mentioned as a primary candidate in limiting the output

power of a laser using highly doped erbium fiber. It was also during these discussions that Dr. Paul Wysocki of Bell Labs graciously agreed to donate a length of erbium doped fiber that had been designed for amplifier configurations. In his estimation, 100 mW of output should be possible with a reasonable length of this more moderately doped fiber.

### 2.5 Final Cavity Design

After investigations of different gain media, detailed in a previous section, the final cavity configuration of Figure 2.3 was constructed. Although this cavity configuration may at first seem complex, it was selected to permit the source to be compact, robust, and easy to use. Optical fiber couplers were inserted into the cavity rather than bulk optics not only because they permitted the source to be compact, but because, after splicing, they require no user alignment - a key element in making the laser easy to use. In order to explain the function of the different components of the cavity, the beam path will be detailed starting from the pump light input.

Bulk optics relay the optical pump from a CW Titanium Sapphire (Ti:S) laser, lasing at 980 nm, to the input of this system where it is coupled into single mode fiber. The input fiber is actually the input lead to a fixed ratio fiber coupler. This coupler splits 10% of the input light and directs it toward a port that has an FC-PC connector fusion spliced to it so that the pump light coupling efficiency can easily be monitored by a fiber coupled optical power meter. The optical fiber containing the remanding 90% of the pump light is spliced to a Wavelength-Division-Multiplexing (WDM) coupler at the short wavelength port. The multiple wavelength port of the WDM coupler is connected to the gain medium - single mode optical fiber doped with the rare earth element Erbium. The pump light is absorbed over the length of the erbium-doped fiber. The light emitted from the erbium fiber due to either spontaneous or stimulated emission is directed primarily in two directions, which I will call simply 'forward' or 'reverse', due to the wave guiding nature of the optical fiber. By way of convention, the 'forward' direction will be considered to be co-propagating with the pump light while the 'reverse' direction will be counter-propagating. The 'forward' directed emission travels from the gain medium to an anti-reflection coated fiber lens, a commercial gradient-index lens packaged with a single mode fiber connection, for free-space propagation to the diffraction grating. The grating

reflects a single wavelength component of the otherwise broadband erbium emission back to the fiber lens while causing loss at the adjacent wavelengths. The fiber lens couples this radiation back into the optical fiber where it proceeds through the cavity in the direction of the 'reverse' erbium emission described earlier. The light traveling in the 'reverse' direction is guided from the multiple wavelength port of the WDM coupler to the long wavelength port. This port of the WDM coupler is spliced to another fixed ratio fiber coupler. This coupler acts as the output coupler would in a conventional bulk optics laser cavity. The low power output side of this coupler, 10% of the input, is spliced to the input of a 50-50 coupler. The output leads of this coupler are spliced together to serve as an optical fiber mirror so that the reflectivity of the output coupler is 10%. The high power port of the output coupler, 90% of the input, is then fusion spliced to an optical isolator so that any light reflected from components further on in the system is blocked from re-entering the cavity and disturbing or modifying the laser performance. The output of the optical isolator is then spliced to a 2X2 coupler with FC-PC connectors fusion spliced on the remaining three ports. This configuration allows either high or low output powers to be directed to the experiment of interest by simply selecting the appropriate output connector as well as permitting the reflection from those end faces to be monitored at the other 'input' port of the 2X2 coupler. The reason for this functionality will be explained in more detail in the measurement system chapter.

### 2.5.1 Optical characteristics

The optical characteristics of the final laser cavity, employing approximately 40 m of erbium doped fiber donated by AT&T are displayed in figures 2.4 and 2.5. The first figure displays the output power as a function of coupled input power for two different wavelengths. As can been seen, nearly 200 mW of output in the 1.55 μm band is possible for reasonable levels of optical pump. The linewidth of the laser action has been measured to be approximately 0.25 nm full width at half maximum and the center wavelength could be determined within +/- 0.1 nm. While far from ideal, these values were determined to be good enough for the purposes of characterizing the AFPM. If decreased linewidth is desired, the most obvious modification to be made is to increase the laser spot size at the

diffraction grating. This would increase the resolution of the system and increase the wavelength selectivity of the cavity feedback thereby decreasing the linewidth.

Output power as a function of wavelength, for a fixed level of pump power is displayed in figure 2.5 in the form of a tuning curve. In order to generate this curve, the laser output is connected to the OSA and the OSA is configured to maintain the maximum signal at each wavelength within the scan range. While this mode is selected, the diffraction grating is rotated in order to trace out the tuning curve. Note that the intensity of the curve displayed is logarithmic. As can be seen, nearly 60 nm of continuos tuning is possible with a relatively constant output power. While this system performance certainly does not break any records in terms of output power or tuning range, its simplicity and robustness have made it into a key characterization component for very little cost.

## 2.6 Final Comments

While it was initially thought that a high power, broadly tunable laser source was necessary as an optical source for the modulator characterization, in fact, functionally, the most important characteristic of this source was its ability to function as a high power white light source in the 1.55 μm wavelength band. This statement has its origin purely in the convenience of the data acquisition of the reflectivity signal.

As a laser system, in order to be used to characterize the spectrally dependent reflection of the asymmetric Fabry-Perot modulator, the laser would need to be tuned to many different wavelengths within its emission band while recording the magnitude of the reflection from the sample of interest. While these measurements are certainly possible, without some sort of automation scheme they tend to be quite tedious. The monotony of these measurements becomes magnified when one considers that they must be repeated at a variety of electrical bias levels.

At the time that optical characterization of the asymmetric Fabry-Perot reflection modulator began, two possibilities to relieve the monotony of the data acquisition were realized. First, the laser source could be modified in order to include a stepper motor driven rotation stage with the diffraction grating tuning element. With the inclusion of some custom written control software, reflection spectra could be taken in a matter of seconds under computer control. While this solution is certainly desirable, at the time

optical characterization was beginning, it was determined that the time necessary to develop the custom control software was probably not a wise investment - particularly since automated data acquisition was possible by simply operating the laser as a broadband white light source by turning the optical pump down to below the lasing threshold.

With a broad spectral band of light impinging on the AFPM, it was possible to characterize the entire spectrally dependent reflection in a single shot by simply coupling the light reflected from the AFPM into an optical fiber and connecting it the optical spectrum analyzer. Regardless of the fact that this scheme certainly has less optical power impinging on the modulator than using the system as a tunable laser, the high sensitivity of the OSA easily enabled the automated data acquisition with no further time investment.

As an aside, the automated tuning and data acquisition of the erbium fiber laser has in fact been carried as of this writing. During the summer of 1996, an Undergraduate from Purdue University, Joseph De Nicholas, created an automated tuning and data acquisition system for the CW erbium fiber laser.

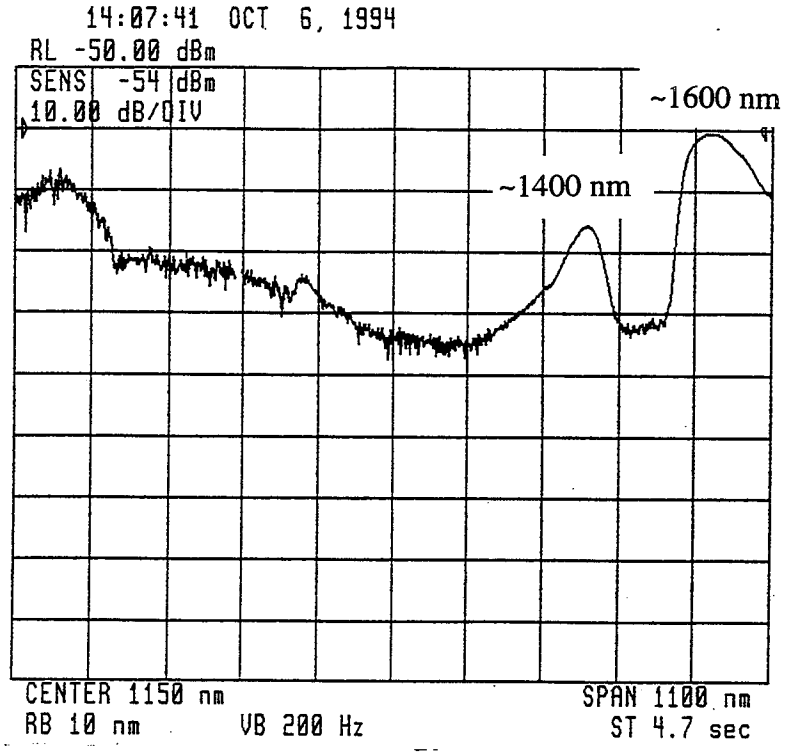


Fig. 2.1. ASE spectrum of 5m of fiber ErCaAl081790-082090

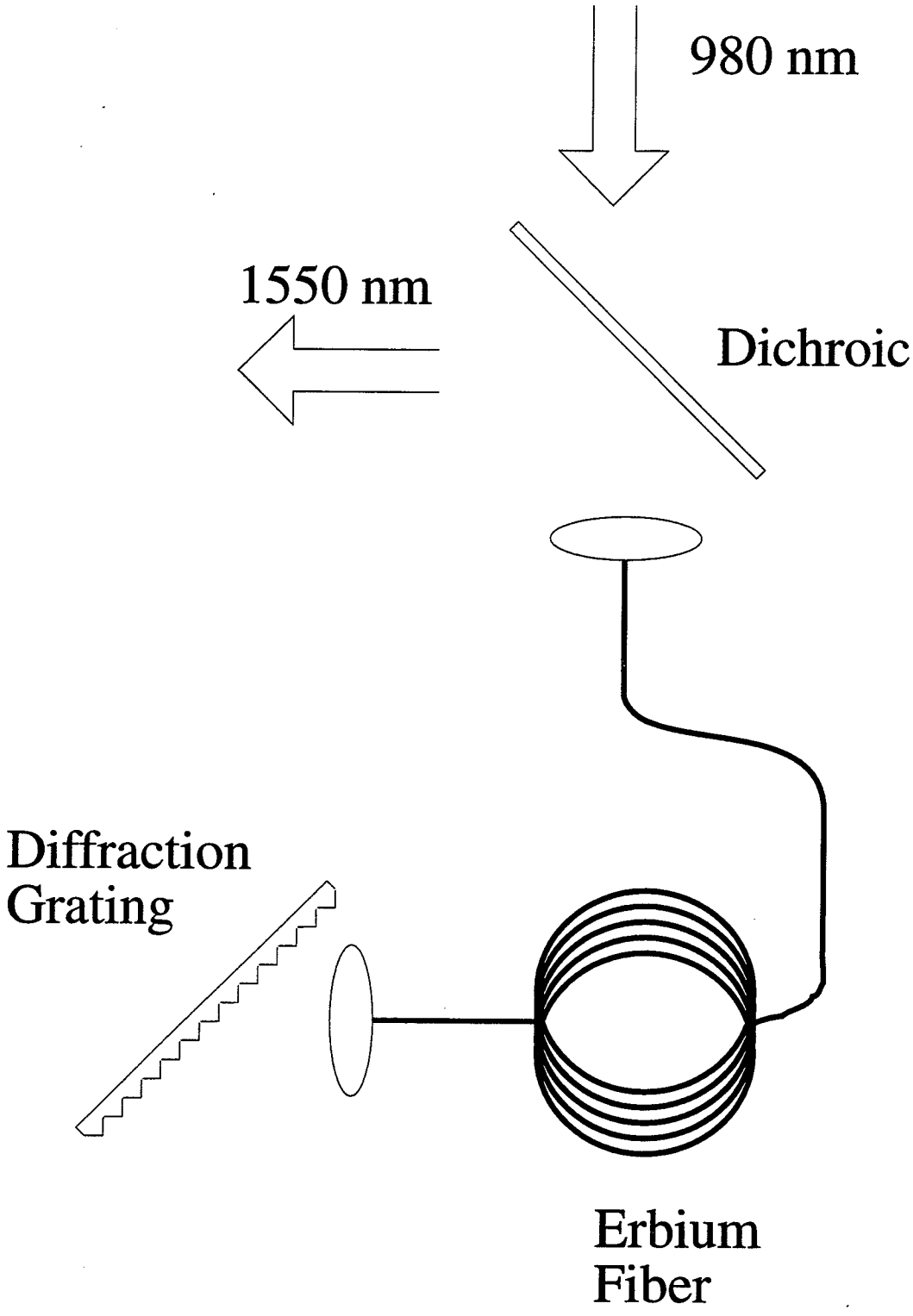


Fig. 2.2. Schematic of the test cavity design.

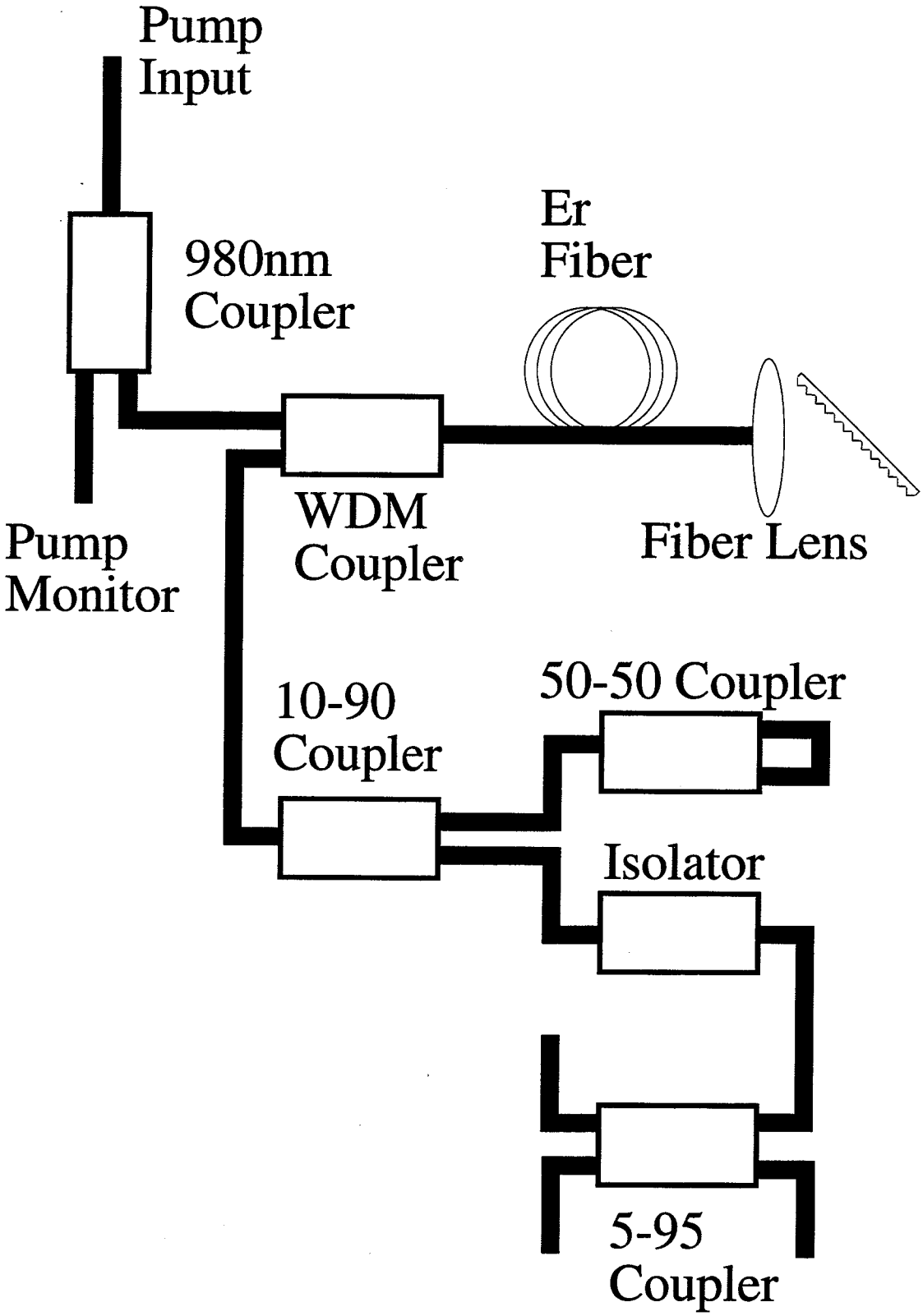


Fig. 2.3. Final cavity design.

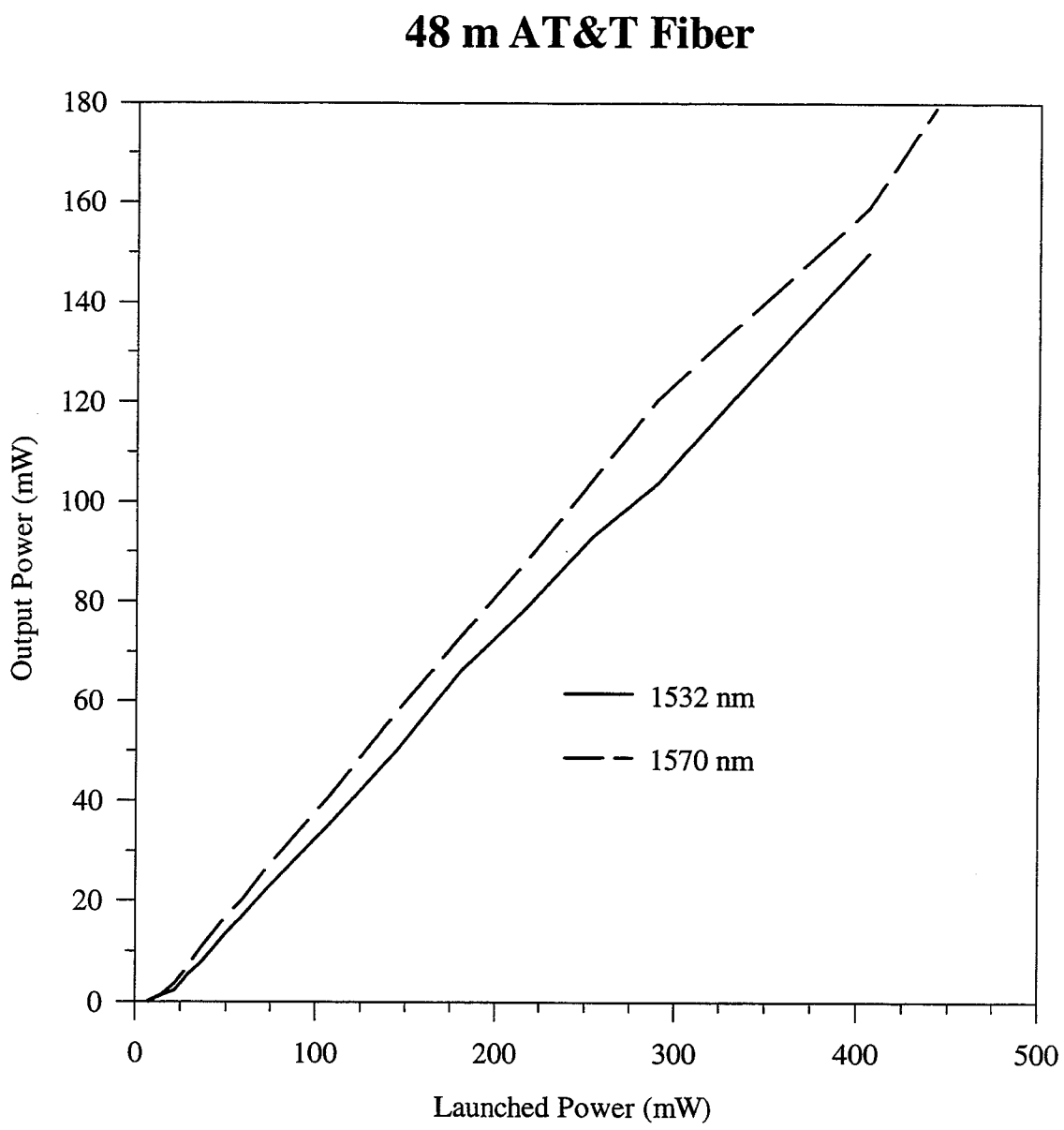


Fig. 2.4. Output power vs. input power for the laser consisting of approximately 40m of AT&T erbium doped fiber.

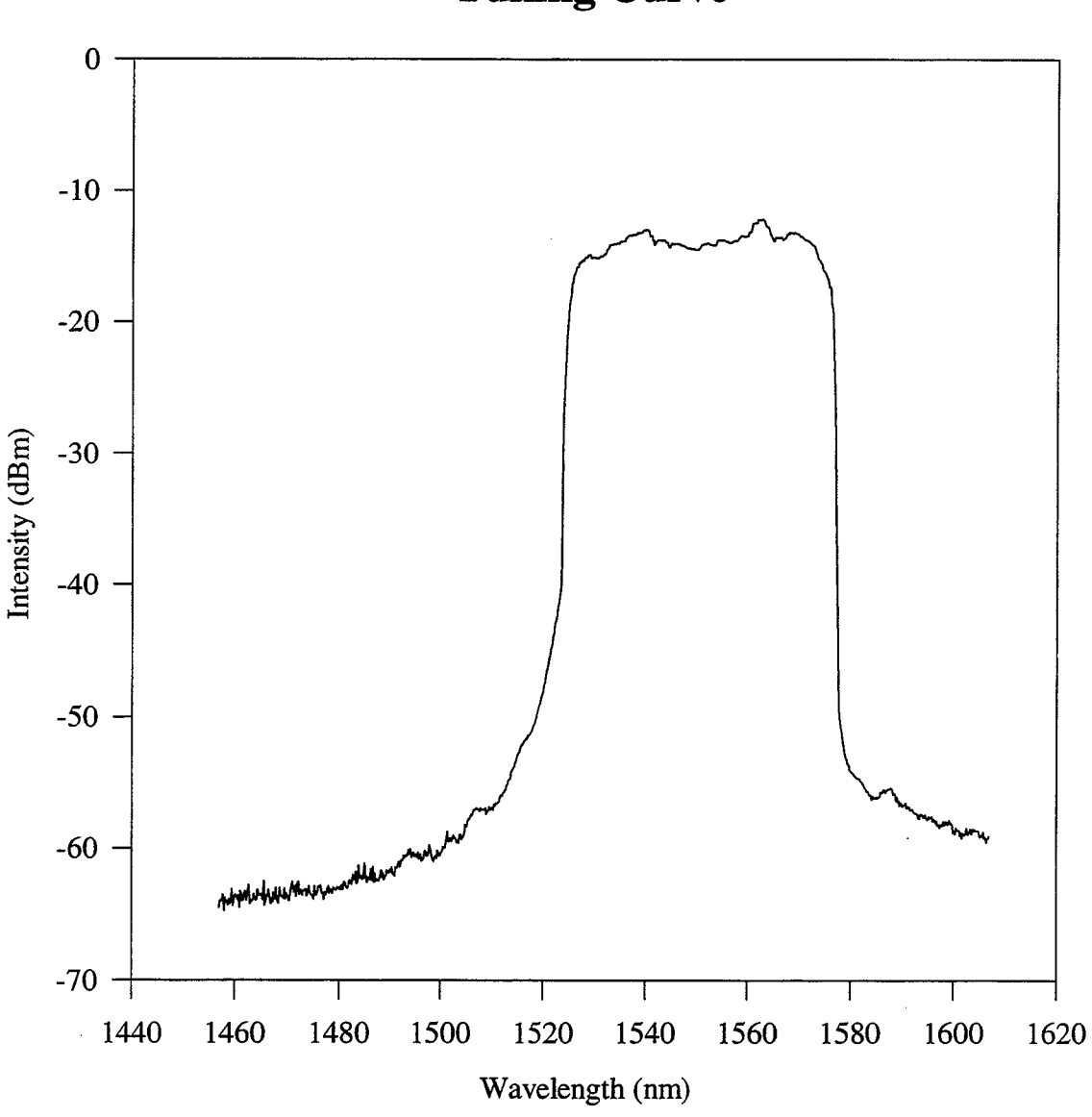


Fig. 2.5. Tuning curve for the laser constructed with the AT&T fiber.

# 3. MODULATOR CHARACTERIZATION

## 3.1 Introduction

As the title of this thesis states, the device to be characterized was an asymmetric Fabry-Perot reflection modulator. For those unfamiliar with this device architecture, a paragraph will be spent on reviewing the attributes of this style of device.

The 'asymmetric' portion of the device style comes from the fact that the outside surfaces of the device, the end mirrors, are mirrors of different reflectivities. The 'Fabry-Perot' portion of the device style indicates that the active region, or the cavity between the two end mirrors is an odd multiple of one half wavelength in extent. In this way, the light reflected from the back mirror can be made to cancel the reflection from the front surface. The on-off state of a Fabry-Perot can be modulated in one of two ways. Either the physical length of the cavity can be modulated; thereby, modulating the resonance wavelength, or some absorption can be introduced into the cavity and modulated off and on. With some absorption in the cavity, the off state corresponds to when there is no, or relatively low absorption so that the reflected wave adds to the wave reflected from the front surface but 180 degrees out of phase. In this way , the reflection is canceled. In the on state, the reflected wave, at best, only partially cancels the wave reflected from the front surface. The extreme on state case is when an infinite absorber is placed into the cavity. In this configuration, the back mirror is not seen at all, and the on state is characterized by the reflectivity of the front mirror.

The Fabry-Perot devices to be investigated here utilize changes in absorption within the cavity in order to modify the reflectivity character of the device. This change in absorption is provided through electro-absorption in which the center wavelength of the absorption feature of a multiple quantum well is red-shifted with applied bias. By carefully constructing the multiple quantum well (in terms of composition and thickness), the

wavelength of the absorption feature can be matched to the resonance of the Fabry-Perot so that a range of absorption is possible within the cavity as a function of applied bias.

The modulators to be characterized in this work were provided by Ben Yoo of Bellcore. In was expected that the modulators would provide characteristics similar to those previously reported [14-15], except for perhaps operating at a longer center wavelength than the earlier work.

In order to characterize the on-off character of a device similar to that just described, three elements are necessary. First, variable wavelength light is necessary so that the reflectivity of the device can be monitored as a function of wavelength. Second, in the case of an electro-absorption based device, electrical bias must be applied in order to change the level of absorption in the cavity and, hence, the device reflectivity. Finally, some mechanical apparatus must be constructed that permits both optical and electrical access simultaneously.

The CW fiber laser system described in the previous chapter served as only the first of two primary enabling devices in the characterization of the asymmetric Fabry-Perot reflection modulator. The second device required to perform the optical characterization was some apparatus that would permit not only optical access for the incident and reflected beam, but electrical access in order to apply the required bias. Very early on in the design of the characterization apparatus, it was decided that only DC biases would be initially applied due to two primary considerations. First, the available sample consisted of not a single device array but an entire section of a wafer with many device arrays of different active areas. The geometry of the loaned sample coupled with the fact that it had never been previously characterized and inexperience with device characterization at 1.55 μm forced a rather simple device characterization apparatus to be initially investigated. If an entire functional array (or at least a major portion of an array), with reasonable DC characteristics, could be identified, the sample would have to be packaged to allow fast electrical signals to be applied. Second, since this section of wafer had not been previously characterized, it was important to determine in what wavelength region the reflectance could be nulled with the application of bias and, correspondingly, what level of

on-off ratio was possible under reasonable reverse bias conditions. These initial investigations could most easily be carried out under DC bias conditions.

### 3.2 Visual Characterization

Prior to constructing some sort of electro-optical characterization apparatus in order to carry out initial investigations of this device structure, the sample was described visually. The purpose of the visual mapping of the sample was to determine if there were any obvious reasons why the electro-optical characterization should not be carried out on a section of the sample.

Using a standard optical microscope, three functionally redundant regions were identified on the sample, as indicated in figure 3.1A. In order to refer to any particular device on the sample, the numbering scheme show in figure 3.1B was adopted. Under this scheme, the three functionally redundant sections of the sample were designated as sections A, B, and C. Within each of these sections, several repetitions of six different modulator sizes were present - each as an array of eighteen modulators of the same active dimension. Each repetition of the six different size modulator arrays was designated as a series (i.e. series 1, series 2, etc.). Within each series, the different modulator sizes were designated as size 1 to size 6 with 6 referring to the largest modulators and 1 referring to the smallest. Finally, modulators were numbered within the array, from left to right, 1 to 18. The modulators themselves are circular in nature with three electrical contacts per modulator configured in a ground-signal-ground configuration. The active areas are separated by 62.5 μm.

Using the naming scheme described above, it was determined that electro-optical characterization should not be carried out on any of the modulators in section A nor any of the modulators in the bottom half of section C due to obvious electrical shorts in the electrical bias lines of the modulators in these sections.

### 3.3 Optical Characterization Apparatus

Now that some sections of the sample were determined to be unacceptable due to the visual character, it was time to start electro-optical characterization of the remaining modulators. Given that the optical source, described in chapter 2, was fiber based, the

initial characterization apparatus was imagined as fiber based as well. Some problems with this geometry, to be detailed shortly, lead away from a fiber based characterization system to a free space optical coupling geometry. However, the initial implementation of this, keeping the device vertical, suffered from some difficulties. Finally, it was determined, for reasons that will be detailed later, that the device should be held in a horizontal position for optimum measurement repeatability. The final electro-optical characterization system was designed and constructed so as to allow the modulator position to be set at the focus of the optical beam with a resolution of +/- 1 μm in all three principal axes. Pitch and yaw controls were also implemented so that the beam reflected from the modulator could be directed exactly back along the input direction. Electrical connections were also made to the modulator through two independent home-made probe tip mechanisms. Finally, all of the previously mentioned controls were mounted so that the modulator, with electrical connections intact, could be moved in all degrees of freedom while monitoring the generated photocurrent so as to optimize the modulator position.

### 3.3.1 Vertical geometry

Initially, since the laser source to be used was fiber based, a fiber coupled optical delivery system was imagined. This configuration was realized by the use of a 2X2 coupler at the laser output. The output of the laser source was connected to an optical isolator so that feedback from the device measurement would not interfere with the laser performance. The isolator output was connected to one of the 'input' ports of the 2X2 coupler. The coupler splits this input into two outputs - one of which is 10% of the input, the other is 90% of the input. The 10% output port was butt-coupled to the modulator array so that light was directed to the modulator and the reflection recollected by the same fiber end. This output port, because of the symmetry of the passive coupler, would then serve as an input to the 2X2 coupler for the reflected beam with 90% of the reflected beam available for monitoring at the unused original input port. The other output port (90% of the laser output power) was available for monitoring the laser performance. This measurement geometry is shown schematically in figure 3.2.

Connecting the secondary input port to the OSA allowed the spectrally dependent reflection to be monitored quite easily. However, several difficulties with this measurement scheme lead to other characterization apparati being considered. The most important difficulty encountered was the repeatability of the measurement.

Since the light was coupled into and out of the modulator by the same piece of optical fiber, the alignment of this fiber relative to the modulator being measured was critical. Not only was the positional dependence quite sensitive, but varying the angle of the fiber end relative to the modulator could cause unusual spectral characteristics to be apparent. These tight alignment tolerances made reflection measurements very difficult to repeat.

Coupled with the alignment tolerance problem was difficulty in interpreting the results. The bare fiber end produces approximately a 4% reflection back into the fiber due to the air - glass interface. This 4% reflection would interfere with the signal of interest from the modulator and another 4% reflection from the 90% output port (actually, only 10% of this second endface reflection would interfere, but its phase relationship would be unknown and vary with temperature and any stress on the fiber lengths). All of these interfering signals conspired to make measurement interpretation quite difficult.

In order to ease the interpretation of the measurement, it was decided to investigate a free space coupled geometry. The first attempt at free space coupling is shown in figure 3.3. In this setup, the output of the fiber laser was collimated by some output coupling optics then relayed through a beamsplitter and focused onto the modulator with a final focus lens. The light reflected from the modulator would be recollimated by this focus lens and then monitored after the beamsplitter. Monitoring the entire reflected spectrum at once could be accomplished by coupling the reflected beam from the modulator via the beamsplitter into an optical fiber and then connecting this fiber to the OSA.

While this characterization scheme eliminated the measurement interpretation problems, effort to fully develop the necessary infrastructure was not expended due to concerns with intermittent electrical contacts. With the modulator mounted in the vertical position, it was noticed that the photocurrent generated during the alignment phase of a measurement would fluctuate over a wide range. Presumably this was due to minute shifts

in the probe tip positions while the modulator position was being optimized. This problem was probably compounded by the rather long (~ 3 inch) and thin (1/32 inch piano wire) probe tips that were in use at the time.

Optimization of the vertical geometry was certainly possible in order to minimize the measurement uncertainties associated with the electrical contacts; however, while the effort was being expended to redesign the probe tip arms and mounting configuration, the decision was made to modify the characterization system even further in the hope of achieving even further stabilization of the intended measurement.

### 3.3.2 Horizontal geometry

The primary concern with the vertical free space coupled geometry was that the electrical character of the system seemed to fluctuate most likely due to probe tip movements on the contact pads owing to the mass of the probe arm and the vertical mounting geometry. In order to eliminate these concerns, the characterization system was modified one final time in order to mount the modulator array in a horizontal fashion with free space coupling. A schematic of the final electro-optical characterization system is shown in figure 3.4. Several design improvements were implemented which radically increased the characterization systems stability and repeatability over that obtainable with the previous characterization systems.

One major improvement that is not visible in the characterization system schematic diagram is the probe tip redesign. In the earlier characterization system implementations, the electrical probe tips were pieces of spring steel nearly 3 inches long, 1/32 inch in diameter with one end ground to approximately a 10 μm tip. The two individual probes were held on independent X-Y-Z translation stages with an electrical insulator between the probe tip and the stage assembly. Due to the long, thin nature of the probes, a large amount of flexure was evident upon sample contact. The flexure made it difficult to evaluate the force of the probe tip on the sample so much so that frequently the probe tips could be seen to move due to vibrations in the surroundings.

In order to maximize the stability of the probes while keeping the small tip size, a two stage probe arm/probe tip assembly was designed. The probe arm was constructed of brass welding rod - 1/8 inch in diameter and nearly 3 inches long. The tip was constructed

of the same spring steel used in the earlier probes; however, it was only 1/2 inch long. The tip was inserted into a hole in the end of the probe arm, and held in place by an 0-80 screw through the side of the probe arm. Using this design, both mechanical stability as well as small tip size was obtainable simultaneously.

The other important features of this final electro-optical characterization system are the high resolution positional controls, X-Y-Z as well as pitch and yaw, that position not only the modulator but the probe assemblies relative to the focus lens. Visual determination of the probe tip placement is possible using a television camera and lens mounted above the final focus lens viewing through the 1.55 μm high reflector that serves to direct the optical beam into and out of the modulator.

### 3.4 Reflectivity Measurements

Now that a stable characterization system had been implemented that permitted repeatable reflectivity measurements to be performed, confidence could be placed in the measurements taken. The final purpose of the entire characterization system design and implementation was to permit repeatable reflectivity measurements to be made so that the modulator characteristics could be determined with confidence.

The benchmark to which this sample was to be compared was results that had been previously reported [14-15]. In his measurements, an on-off ratio of greater than 15 dB was reported within a 10 V bias swing at a center wavelength of 1535 nm. An example of these data are given in chapter 4 which discusses modeling of these devices. Ben also reported high speed tests of individual modulators - with a measurement instrument limited modulation rate of 20 GHz, but has not yet reported operation as an array of modulators. For the purpose of these measurements, if even a partial row (of the possible 18 modulators in a row) of modulators could be determined to have reasonable on-off ratio characteristics, quite interesting optical pulse shaping experiments could be imagined after packaging the device into an array.

Unfortunately, optical characterization of these modulators was hindered by a large number of the modulators exhibiting characteristics of an electrical short. In these modulators, as the magnitude of the electrical bias was increased, the current would radically increase. Conversely, in modulators that did not exhibit the electrical short

character, the current generated with light incident on the modulator, the so called photocurrent, would increase nearly linearly with the magnitude of the applied bias. In these 'good' modulators, the character of the optical reflection could be seen to change as the applied bias was increased while the 'bad' modulators showed no change in reflectivity.

Simply as a means of documentation, the procedure for making a reflectivity measurement on an individual modulator was as follows. First, with the electrical bias turned to zero, the probe tips were positioned on the modulator of interest. While connections on the modulator were available in a ground-signal-ground configuration, only a single ground was used in these DC measurements. The signal pin was connected to a power supply so that variable negative biases could be applied.

The first adjustment of modulator position did not rely at all on the applied electrical bias. The pitch and yaw controls of the modulator assembly were adjusted so that the beam reflected from the modulator was directed directly back upon the input. This alignment was confirmed by closing down the iris shown in figure 3.4. The power measured after the beamsplitter was maximized by adjusting the pitch and yaw controls. Any angular misalignment of the reflected beam relative to the input could easily be eliminated using this scheme. After the angular controls were set during any particular measurement session, they were typically not adjusted further.

With the angular controls set, the next step was to couple a visible helium-neon (HeNe) laser into the optical fiber connected to the fiber lens. Using this visible light, the position of the modulator stage was set to where the HeNe beam was roughly centered on the modulator of interest. The positioning could only be set roughly since the optical fiber used was single mode at 1.55 μm, but multi-mode at the 0.632 μm HeNe wavelength. Now that the modulator position was coarsely set, the visible light was disconnected and the light from the CW erbium fiber laser was connected to the fiber lens pigtail. Typically, some photocurrent was evident at this time for a modest magnitude of electrical bias (around -5 V). The position of the modulator stage was then adjusted, in X, Y, and Z in order to optimize the measured photocurrent. All of the photocurrent based adjustments were made with the characterization source acting as a laser.

Finally, with the position of the modulator optimized, the diffraction grating component of the characterization source was blocked and the pump power adjusted in order to give the maximum amount of ASE available from the source without it actually lasing. The electrical bias was set to 0 volts, and an optical reflectivity spectrum was recorded over the range of roughly 1.520 μm to 1.580 μm in a single shot using the OSA. The magnitude of the negative bias was then increased, and the reflectivity measurement was repeated. Examples of reflectivity spectra taken at 0 and -10 V bias conditions are shown in figure 3.5. Note that these spectra are logarithmic in intensity.

In order to determine the change in reflectivity versus applied bias, the recorded intensity spectra were converted to linear scales and the zero bias trace was divided by the biased case in post measurement processing. A typical change in reflectivity curve is shown in figure 3.6 for a ten volt swing. Several general trends in these measurements should be mentioned at this time. First, the full-width-at-half-maximum (FWHM) of the dip in reflectivity tends to be approximately 9 nm. Second, the center wavelength of this dip changes nearly linearly with modulator position across the sample from 1.570 nm at one extreme to 1.580 nm at the other. This systematic variance in the center wavelength is evidence of a thickness variation across the sample. As will be seen in chapter 4, thickness variation is a critical parameter in the design and implementation of Fabry-Perot devices. Finally, the largest reflectivity change measured was only 50%, or 3 dB. Comparison of these results with those previously published will be carried out in the modeling chapter.

While the FWHM of the reflectivity change and the range of center wavelengths provide some encouragement for the use of these devices as an array, the maximum measured on-off ratio does not. While much has been learned about the DC characterization of devices such as these, actual optical pulse shaping experiments utilizing these devices is not to be carried out in the near future due to the low contrast and the large number of inactive devices on this sample. If other samples were to be forthcoming, DC characterization could be carried out in a straight forward manner; however, that seems unlikely at this time.

On one final note, even though the contrast of the present devices is far from ideal, much can be learned about the character of these devices using some rather simple modeling. The results of this modeling is presented in the next chapter.

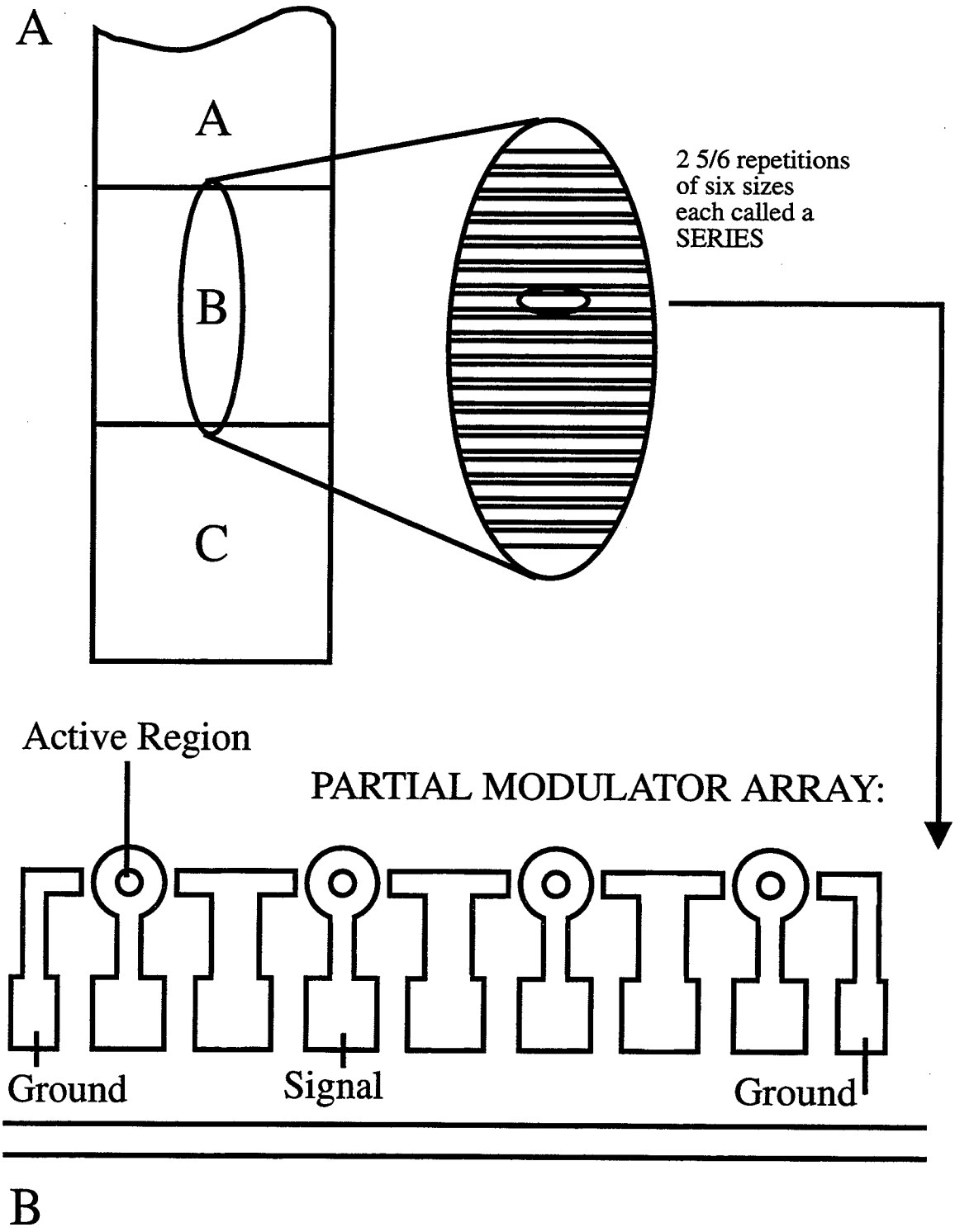


Fig. 3.1. Sample layout (A) and numbering scheme (B).

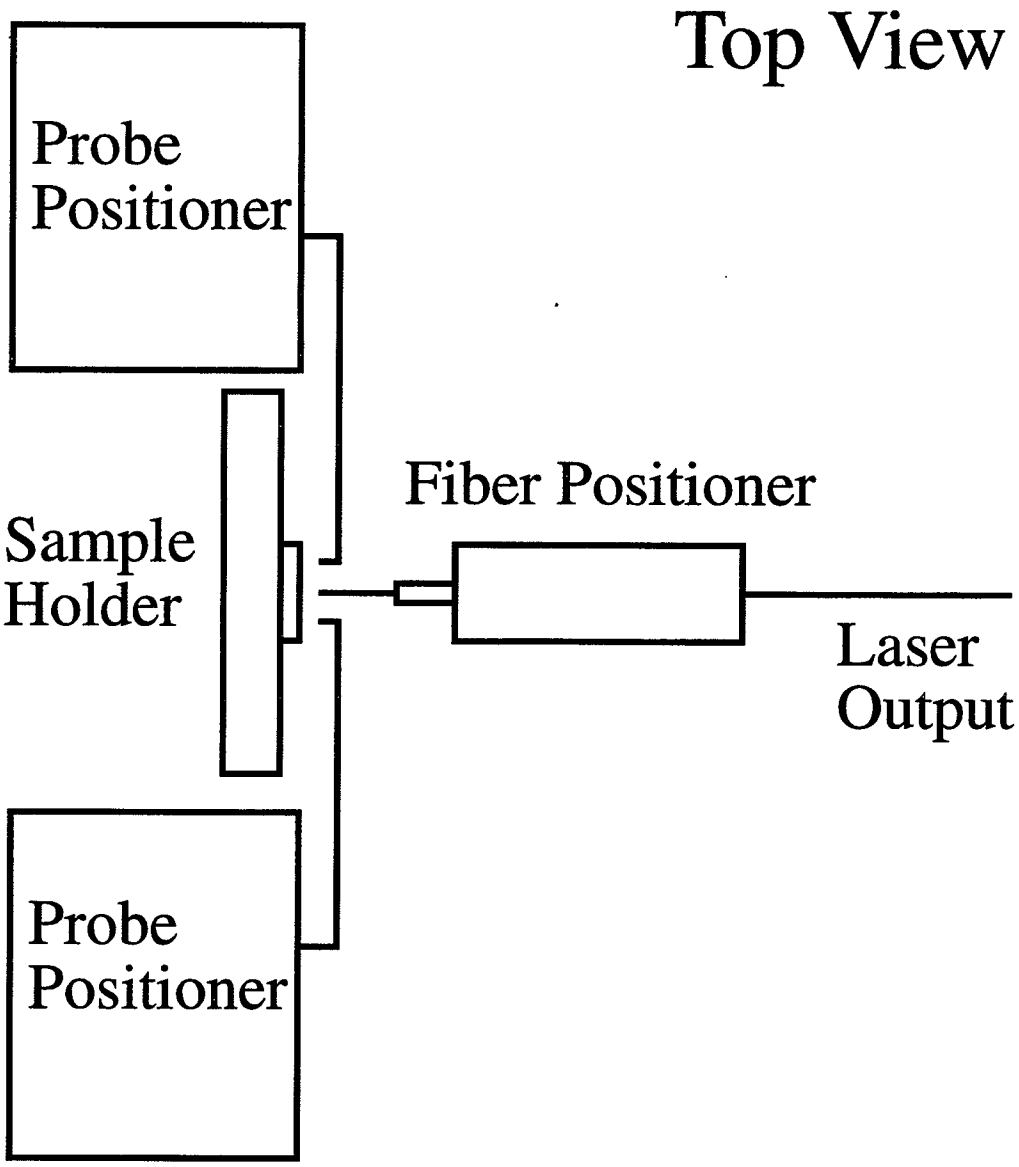


Fig. 3.2. Optical fiber based measurement system.

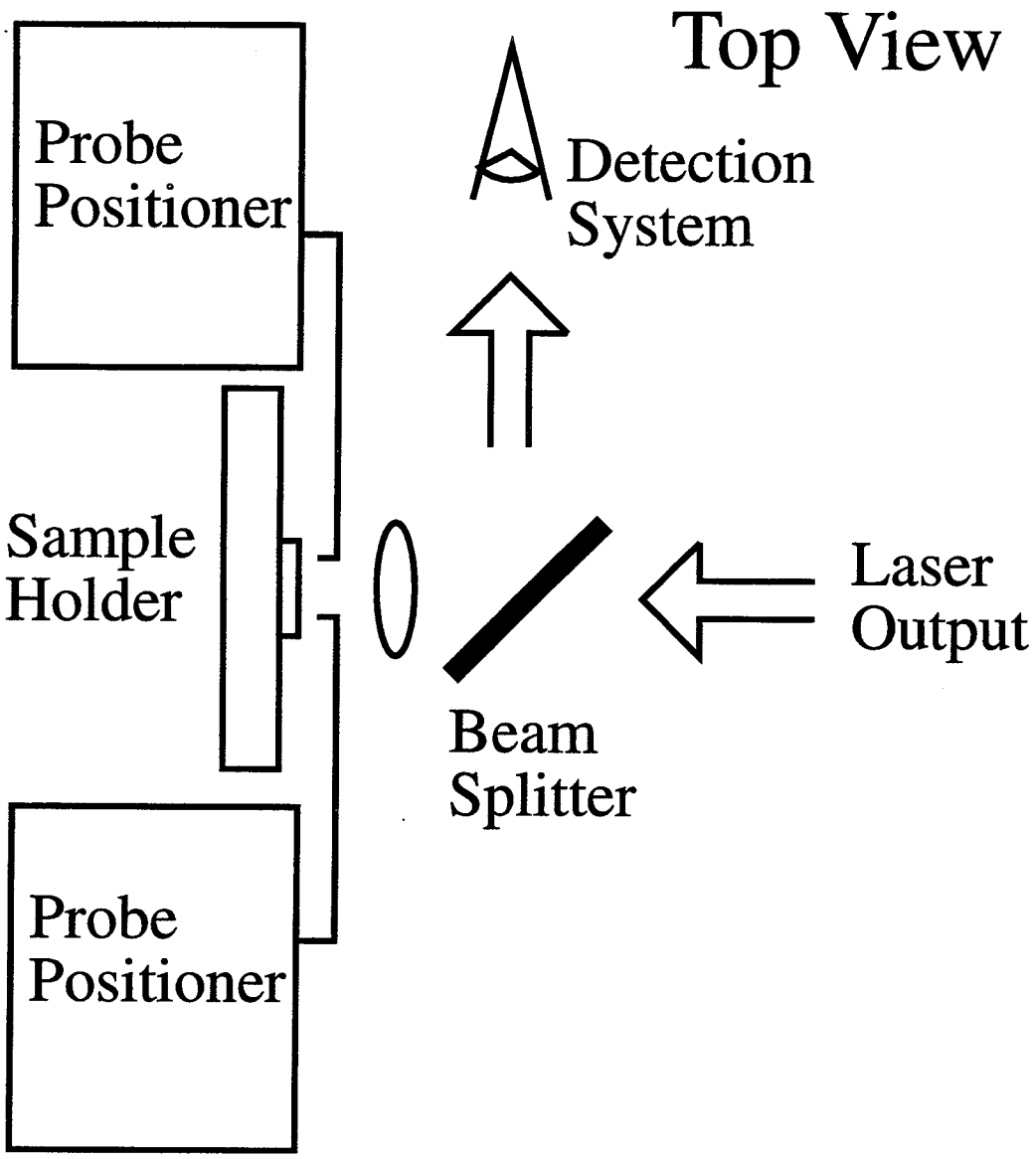


Fig. 3.3. Free space coupled geometry withthe sample vertical.

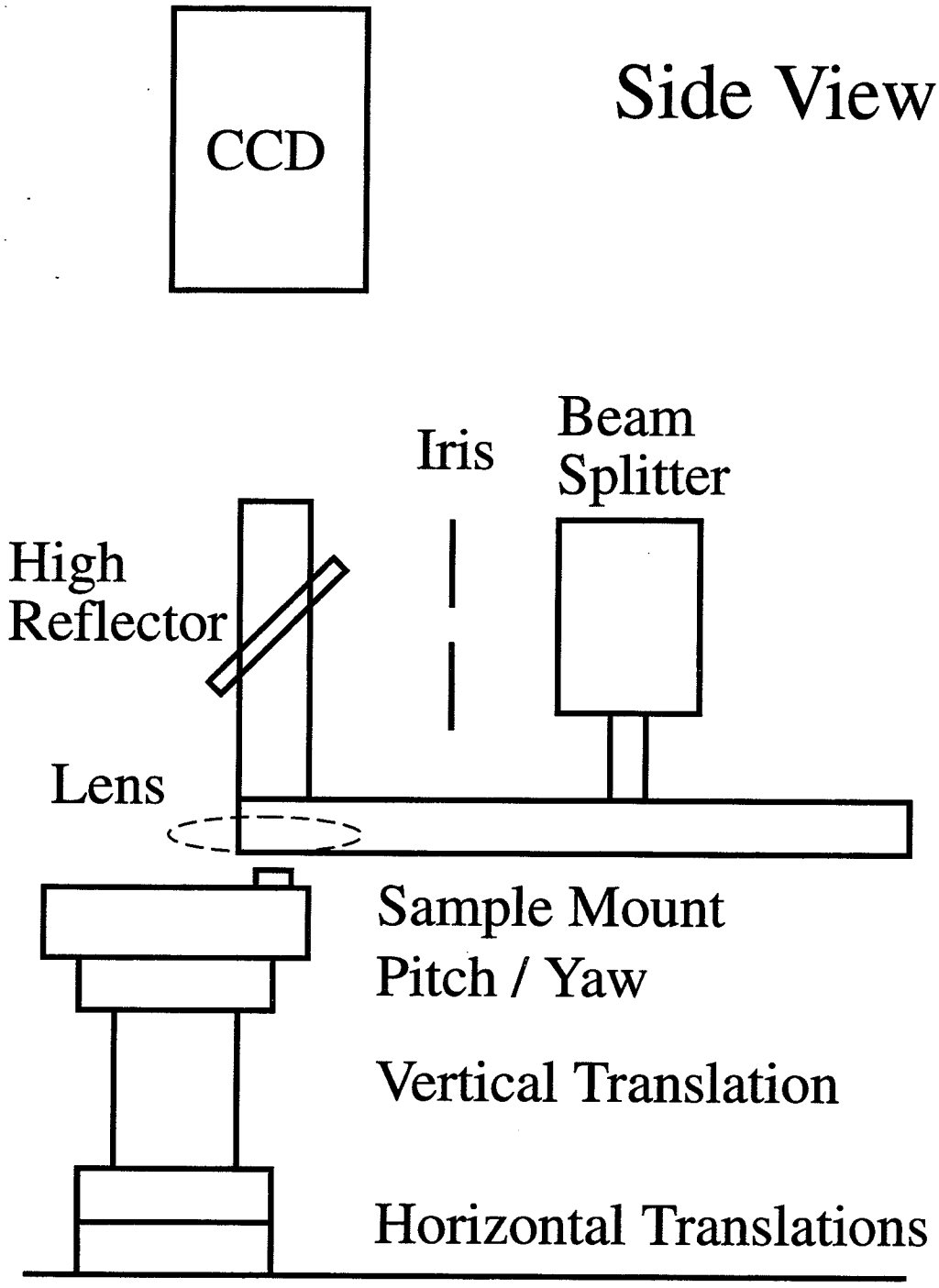


Fig. 3.4. Final characterization system.

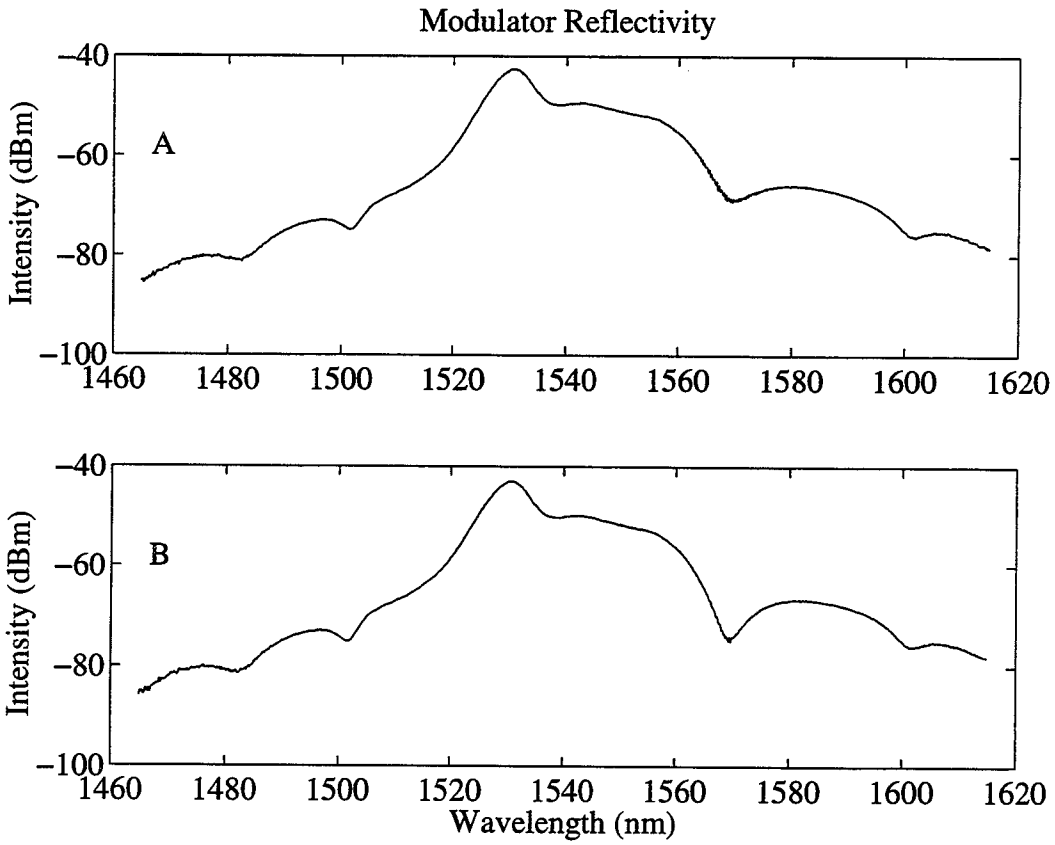


Fig. 3.5. Reflectivity spectra at 0 bias (A), and -10V bias (B).

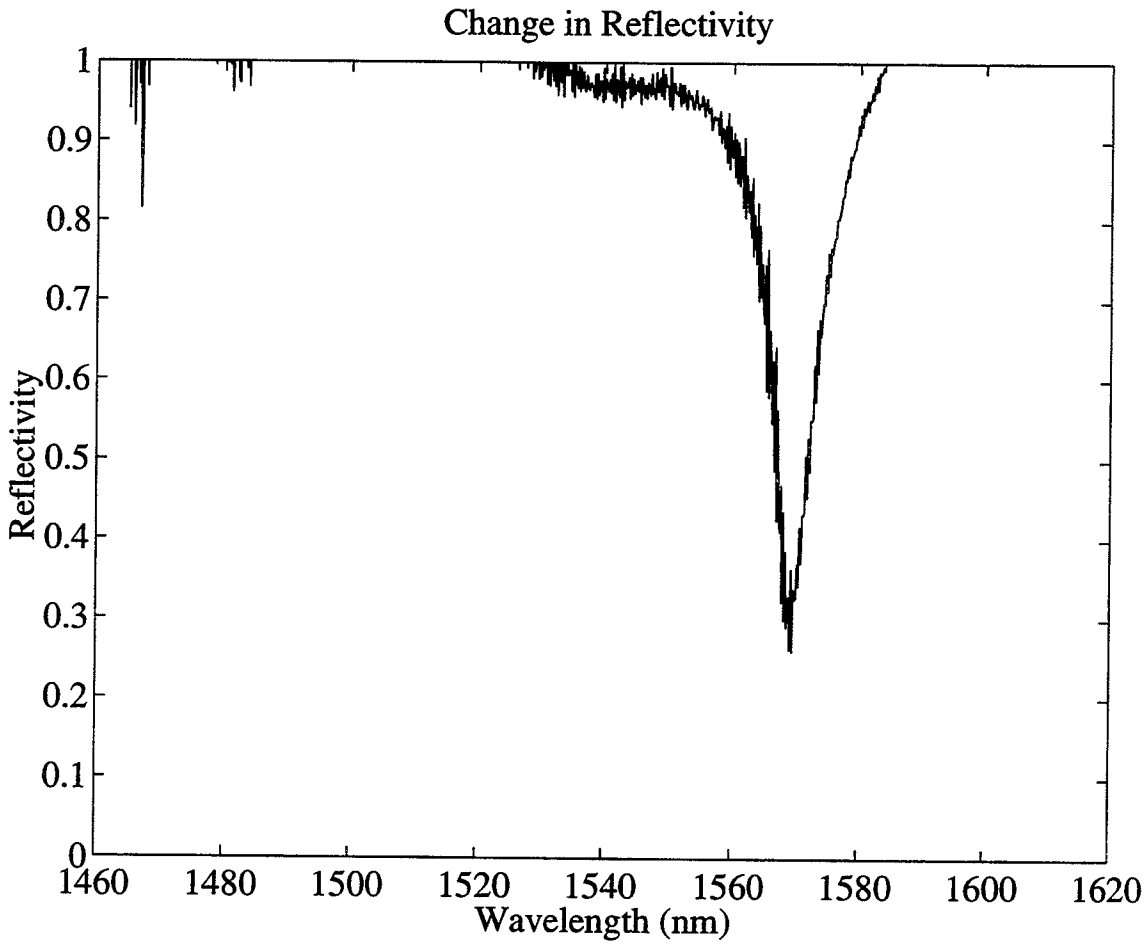


Fig. 3.6. Change in reflectivity.

# 4. MODULATOR MODELING

## 4.1 Introduction

Given the large discrepancy of the measured results compared to those previously published, one would consider whether the measurement was flawed or the device had some difficulty. Much effort was expended developing the characterization system detailed in the previous chapter in order to increase confidence in the measurement. Due to this effort, and perhaps some bias, an attempt to explain the suboptimal results through modeling of the structure was initiated.

The bulk of this chapter walks through the steps taken in developing the modulator model. The sections are organized in much the same order as the thought process that created the final model. Finally, in the last section, the results of the model calculation are directly compared to the previously published data and the reflectivity data taken on the current device. With simple changes to the model, it is easy to show the origin of the decreased measured contrast. These calculations also serve to provide insight into the tolerances necessary to fabricate these devices in a repeatable fashion.

## 4.2 General Procedure

As is actually the case, the device structure is considered to be composed of a series of layers of different thickness and composition. The impedance of the entire structure is calculated from the thickness of the different layers and their refractive index in much the same way as the impedance of a series of transmission lines is calculated [16]. For simplicity, the entire structure is first assumed to be non-absorbing. In the final model, absorption is taken into account by including experimental absorption data into the imaginary refractive index. Using the total effective impedance of the structure, a reflectivity coefficient is determined so that the intensity reflectance of the device can be calculated. For the sake of completeness, relations for the wavelength dependent

refractive index of the various component materials were located and included in the model.

The layer structure of the asymmetric Fabry-Perot reflection modulator is shown in figure 4.1. However, before considering this complex structure, consider the simple three layer structure shown in figure 4.2 in order to summarize the calculation process [16].

The reflectivity at z = 0 is desired, and the impedances of the three layers, $\eta_i$ as well as the thickness, l, of layer 2 is considered known. For simplicity, layer three is considered to be of infinite extent, and the propagation direction is considered to be normal to the layer boundaries.

Using the relation

$$Z_i = \eta_i \frac{Z_L \cos(k_i l_i) + j \eta_i \sin(k_i l_i)}{\eta_i \cos(k_i l_i) + j Z_L \sin(k_i l_i)}$$

the impedance of the structure can be calculated one layer at a time starting with the right most (or farthest in) and working left (or toward the front). In this equation, the subscript i refers to the current layer, the subscript L refers to the impedance of the structure to this point, $l_i$ is the thickness of layer (i), and $k_i$ is the wavenumber, $2 \pi n_i / \lambda$.

Now, starting in layer three, the impedance of layer 3, $Z_3 = \eta_3$. Then, employing the above relation for the effective impedance.

$$Z_2 = \eta_2 \frac{Z_3 \cos(kl) + j \eta_2 \sin(kl)}{\eta_2 \cos(kl) + j Z_3 \sin(kl)}$$

At this point, the effective impedance of this simple structure is known, and the reflection coefficient, at z = 0, can be calculated from:

$$\rho = \frac{Z_2 - \eta_1}{Z_2 + \eta_1}$$

The reflectivity is calculated by squaring the reflection coefficient, $\rho$, from above.

This simple procedure can be followed to calculate the reflectivity of a more complex structure, such as the asymmetric fabry perot reflection modulators, by simply iterating on the calculation of $Z_i$. The only missing component is the relationship between impedance and refractive index which can be given by:

$$\eta = \frac{1}{n}\sqrt{\frac{\mu_0}{\varepsilon_0}}$$

Assuming that $\mu = \mu_0$.

### 4.2.1 Refractive index relations

In order to carry out the required calculations, the relationship between refractive index and wavelength must be known for each material in the structure. The results of literature searches into the refractive index relations of the various materials in the AFPM structure are detailed in the following sections according to the material.

4.2.1.1 InP

From OSA Handbook of Optics, Volume II [17] for $\lambda$ = 0.95 μm to 10.0 μm in units of microns:

$$n^2 = 7.255 + \frac{2.316\,\lambda^2}{\lambda^2 - (0.6263)^2} + \frac{2.765\,\lambda^2}{\lambda^2 - (32.935)^2}$$

4.2.1.2 InGaAsP

In this quaternary compound, the refractive index is dependent of the mole fraction of the various components, x and y, as in $In_{1-x}Ga_xAs_yP_{1-y}$. In order to simplify matters, and since this compound is alternated with layers of InP in the AFPM structure, the relation between x and y was chosen so that the compound would be lattice matched to InP. The lattice matching condition is given by [18]:

$$x = \frac{0.1894\,y}{0.4184 - 0.013\,y}$$

The refractive index is given by:

$$n^2 = 1 + \frac{E_d}{E_o} + \frac{E_d\,E^2}{E_o^3} + \frac{\zeta\,E^4}{\pi}\ln\left(\frac{2E_o^2 - E_g^2 - E^2}{E_g^2 - E^2}\right)$$

With the above variables given by:

$$E_g = 1.35 - 072\,y + 0.12\,y^2$$

$$E_o = 0.595\,x^2(1-y) + 1.626\,x\,y - 1.891\,y + 0.524\,x + 3.391$$

$$\zeta = \pi E_d / 2 E_o^3 (E_o^2 - E_g^2)$$

$$Ed = (12.36\,x - 12.71)\,y + 7.54\,x + 28.91$$

$$E = 1.240/\lambda$$

Once again the wavelength, $\lambda$, is given in microns.

4.2.1.3 InGaAs

In order to keep InGasAs lattice matched to InP, the mole fraction must be $In_{0.53}Ga_{0.47}As$ [19]. Using the lattice matched condition, the refractive index is given by [20]:

$$n^2 = 1 + \frac{64.1508}{(2.5105)^2 - (hv)^2}$$

Note that since this element is the absorptive element within the AFPM structure, the index indicated above corresponds to the real portion, $n_r$, of the refractive index only. The imaginary portion of the refractive index, $n_i$, obtained from the Kramers-Kronig relations will be discussed in a later section. The total index will be a combination of the real and imaginary parts according to:

$$n = n_r - j\,n_i$$

4.2.1.4 AlInGaAs

$Al_xIn_{1-x-y}Ga_yAs$ can be lattice matched to InP over a range of mole fractions through the lattice matching condition [21]:

$$0.468 = 0.983\,x + y$$

Fortunately, guidance was provided by one of Ben Yoo's publications [14] concerning the AFPM. In this publication, it was noted that the bandgap wavelength of this material was 1.25 μm. Using this knowledge, and the relation for the bandgap (in eV) versus mole fraction:

$$E_g(x,y) = 0.36 + 2.093\,x + 0.629\,y + 0.577\,x^2 + 0.436\,y^2 + 1.013\,x\,y - 2.0\,x\,y\,(1-x-y)$$

The specific composition of interest can be calculated to be $Al_{0.19}In_{0.53}Ga_{0.28}As$.

Now that the mole fractions, x and y, are known, the refractive index can be calculated from [22]:

$$n^2 = A_o \left\{ f(\chi) + \frac{1}{2}\left[\frac{E_o}{E_o + \Delta_o}\right]^{3/2} f(\chi_{so}) \right\} + B_o$$

with

$$f(\chi) = \chi^{-2}\left[2 - (1+\chi)^{1/2} - (1-\chi)^{1/2}\right]$$

$$\chi = \frac{\hbar\omega}{E_o}$$

$$\chi_{so} = \frac{\hbar\omega}{(E_o + \Delta_o)}$$

$$E_o = 1.424 + 1.455\,x + 0.191\,x^2 + 1.614\,y + 0.55\,y^2 + 0.043\,x\,y$$

$$\Delta_o = 0.3\,x + 0.43\,y + 0.34\,(1 - x - y)$$

$$A_o = 2.9715 + 11.6407\,x + 1.5749\,y$$

$$B_o = 8.7279 + 10.2892\,x + 4.62578\,y$$

### 4.3 Distributed Bragg Reflector Results

The first attempt at modeling the AFPM was to model the back mirror stack. In a previously published paper [14] on the modulators' performance, it was mentioned that the mirror stack had a 1.535 μm center wavelength, a bandwidth of approximately 100 nm, and a reflectivity of greater than 99%. It was also mentioned that the stack consisted of 42.5 pairs of InP/InGaAsP, but the thickness of the layers was not indicated; therefore, the layers were assumed to be of quarter wavelength thickness at the indicated center wavelength.

In order to test the general procedure of layer impedance calculations as outlined earlier, the reflectivity of the mirror stack alone was calculated. The results of this calculation is shown in figure 4.3. As can be seen, the calculated center wavelength, bandwidth and reflectivity agree quite well with the previously reported values. This calculation gives a large level of confidence in the calculated refractive index relations and the effective impedance calculation procedure.

### 4.4 Full Cavity

With the confidence that the effective impedance calculation seemed to be working properly, it was time to calculate the reflectivity of the entire structure. Initially, the reflectivity of the entire structure was calculated without taking into account absorption effects; then, absorption was added in through the imaginary refractive index of InGaAs.

The imaginary refractive index was calculated using [23]:

$$n_i = \frac{\lambda \alpha}{4 \pi}$$

Where $\alpha$ is the absorption coefficient obtained from the transmission spectra of the multiple quantum well structure according to

$$\frac{I}{I_o} = \exp(-\alpha d)$$

Where $I/I_o$ is the transmission through the sample, and d is the sample thickness.

The absorbence of 80 periods of the multiple quantum well used in the AFPM was published previously [14] and this data, shown in figure 4.4, was scanned and digitized in order to generate the absorption coefficient versus wavelength. The absorbence was defined in this paper to be $-\log_{10}$(Transmission). Since no information was available concerning the exact absorption character of the current sample, and it was known that the center wavelength shifted as one sampled devices across the sample, it was necessary to consider that the exact wavelength of the primary absorption feature may be different than that which was published. Further, other sources of information [24] clearly showed that the wavelength of the absorption feature tends to increase with applied electrical bias. Since no electro-absorption data was available on the current sample, an estimate of wavelength shift needed to be made in order to simulate the device character under bias. Other features were also present in electro-absorption data in the published literature, such as a decrease in the magnitude of the absorption and a broadening of the absorption edge with increased bias; however, these effects were neglected in order to simplify the model. Justification for neglecting these rather important effects will be mentioned later.

As a reasonable starting place, it was decided to attempt to model the previously published results of the AFPM devices. The logic behind this decision was that if these results could be reasonably modeled then the nonideal behavior of the current sample should be able to be explained with some simple modifications to the model. In order to

determine where the absorption edge should be placed, versus wavelength, within the cavity, the published reflectivity results were examined [14]. The primary feature to note is that at 0 bias, the absorption dip in the middle of the mirror stack reflectivity band shows a base reflectivity of nearly 60% while at -10 V bias the reflectivity decreases to exhibit the reported 15 dB on-off ratio. This change in reflectivity is caused by a shift in the absorption edge with increasing electrical bias.

In the on state, at 0 bias, the absorption is relatively high - high enough that little of the light gets through the absorber to reflect back out. In the off state, the absorption is decreased so that light with frequencies within the resonance band of the Fabry-Perot gets through the absorber and adds destructively to the incident field thus nulling the reflectance and creating a large on-off contrast. In order to estimate the position of the absorption edge in these two extreme bias conditions, a simple model of an asymmetric Fabry-Perot cavity with variable absorption was created based on the results of [25].

In this case, the refractive index of the cavity was considered to be a weighted average of the refractive indices of the materials in the actual cavity. The reflectivity of this simple cavity was plotted versus wavelength for a range of absorption -- $\exp(-\alpha d) = 0$ to 1 as shown in figure 4.5. The back mirror reflectivity was taken to be 0.99 and the front mirror reflectivity was taken to be that of an InP-air interface -- 0.27. From this simple model, it was possible to determine that the absorption in the on state was approximately 90% while the off state absorption was approximately 50%. Finally, from these absorption values, it was possible to determine the approximate position of the absorption edge in the unbiased and biased cases. This shift of the absorption edge was taken into account in the final model in order to attempt to duplicate published results.

## 4.5 Experimental Comparison

Figures 4.6 and 4.7 show two comparisons of the model described above with the published reflectivity data. In order to generate the unbiased case, the absorption edge was blue shifted 36.5 nm relative to the published absorbence data while, in the biased case, the edge was red shifted 16.3 nm relative to the published data. As can be seen, the calculated reflectivity curves match very closely the experimental results. The on-off contrast is calculated to be 15.3 dB -- in close agreement with the measured 15 dB contrast. The major discrepancy in both cases is apparent at the extremes of the plot. In the oscillatory tail of the mirror stack, the measured and calculated reflectivities are out of sync by as much as a half period. While the agreement within the central reflectivity band is excellent, this discrepancy in the tail shows that some miscalculation is occurring in the model.

The discrepancy between the model and the experiment can most probably be explained by a lack of information on the exact material composition of the InGaAsP in the mirror stack. The material was taken to be lattice matched to InP, which is probably a reasonable assumption, but it is unclear if this is the case or not. If the mole fraction were adjusted in the model, the refractive index would be modified, and the agreement with the experiment may be able to be improved. However, this effort has not been expended at this time due to the excellent agreement between the model and the experiment within the central reflectivity band - which is where is device is actually operated.

Now that the model has been shown to very reasonably predict the operation of the AFPM under typical operating conditions, modifications need to be made in order to attempt to explain the sub-optimal contrast seen in the current device. Since this device is a Fabry-Perot, it follows that the most reasonable modification that could affect device performance is an error in the cavity length. In order to investigate the magnitude of the performance degradation due to a change in the cavity length, the thickness of the various layers that make up the AFPM cavity were systematically altered - all other parameters were left unchanged.

Figure 4.8 shows the results of an increase in the cavity length of 2%. As can be seen, the center wavelength of the on-off contrast feature has moved to longer wavelengths, and the contrast ratio has decreased by nearly 8 dB as compared to the previous result. Clearly, this relatively small cavity length change indicates that this parameter is critical to the optimum performance of the device. This conclusion should not be unexpected given reports of other devices [26] that actually make use of a thickness variation across the surface of the wafer.

In an attempt to explain the decreased contrast ratio of 3 dB that was measured with the current device, the cavity length within the model was increased even further. Figure 4.9 shows the model results at a cavity length of 4.5% over the optimum case. The experimentally measured on-off contrast for a -10 V bias is plotted on the same graph for comparison. The close agreement between the measured and calculated contrast obviously explain the sub-optimum device performance that was measured with the current sample. As a final sanity check, figure 4.10 shows the calculated reflectivity of the AFPM for a range of biases from 0 to -10 V.

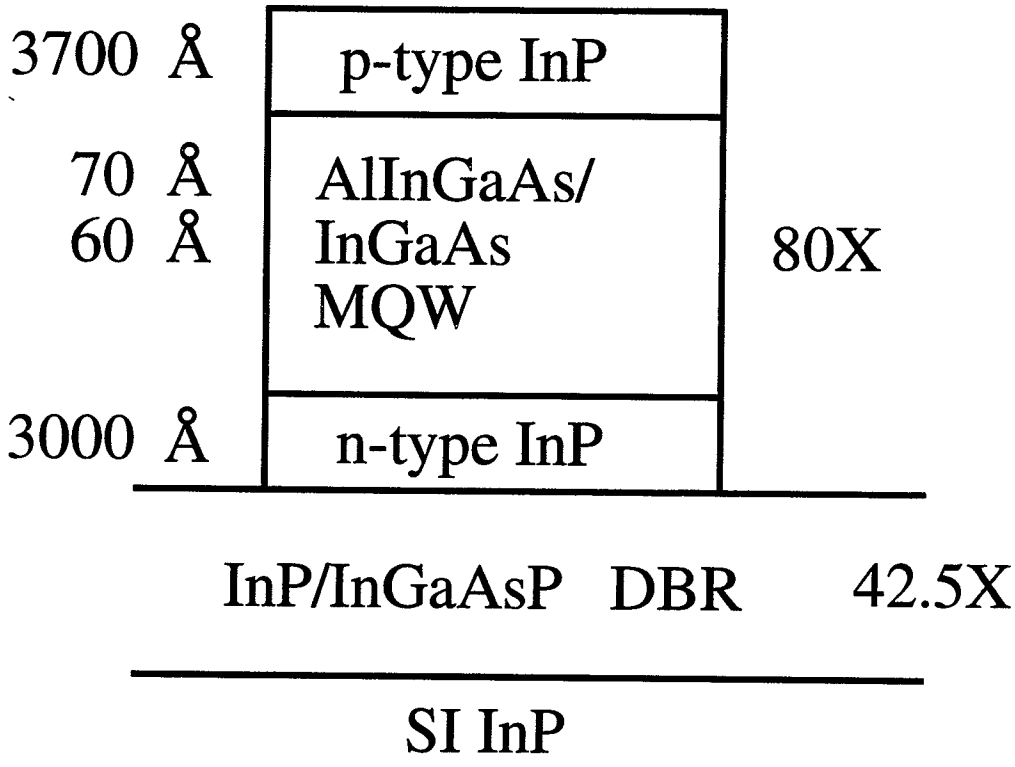


Fig. 4.1. Layer structure of the asymmetric Fabry-Perot.

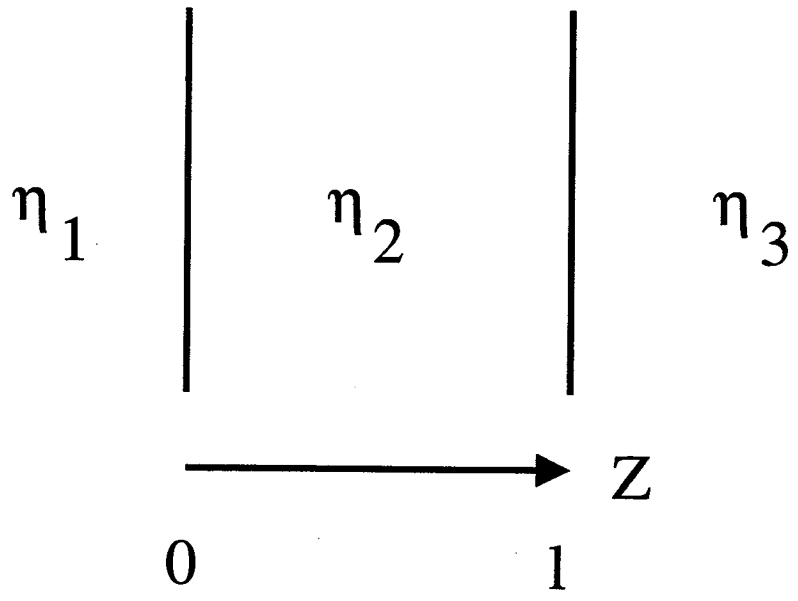


Fig. 4.2. Example effective impedance calculation structure.

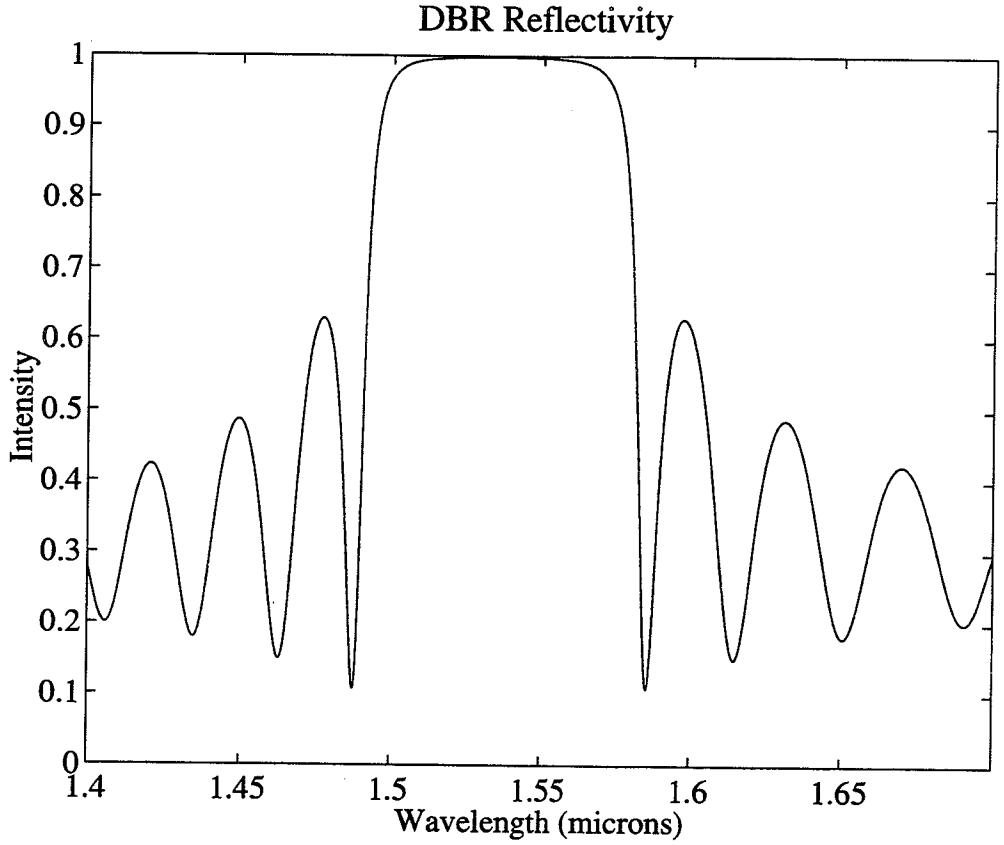


Fig. 4.3. Calculation of DBR reflectivity.

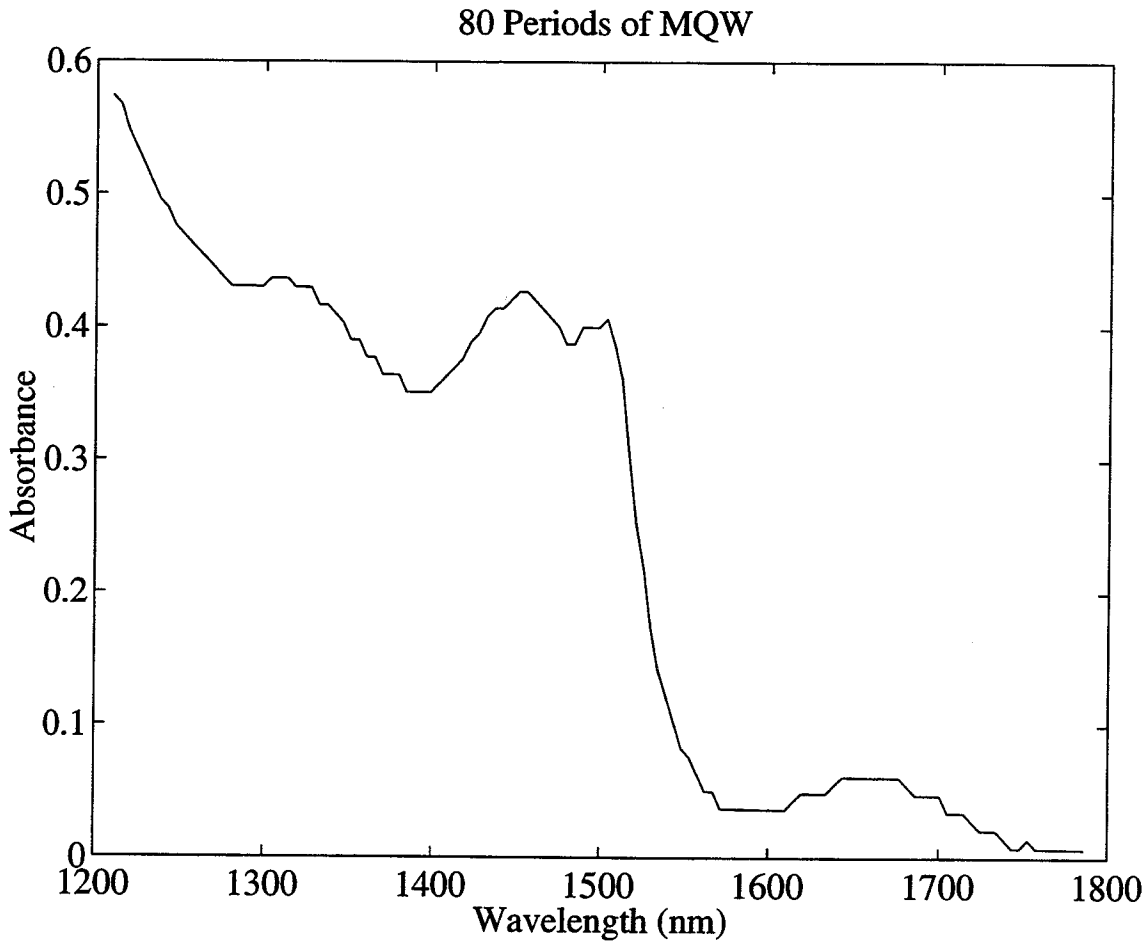


Fig. 4.4. Absorbence of 80 periods of the InGaAs / AlInGaAs MQW.

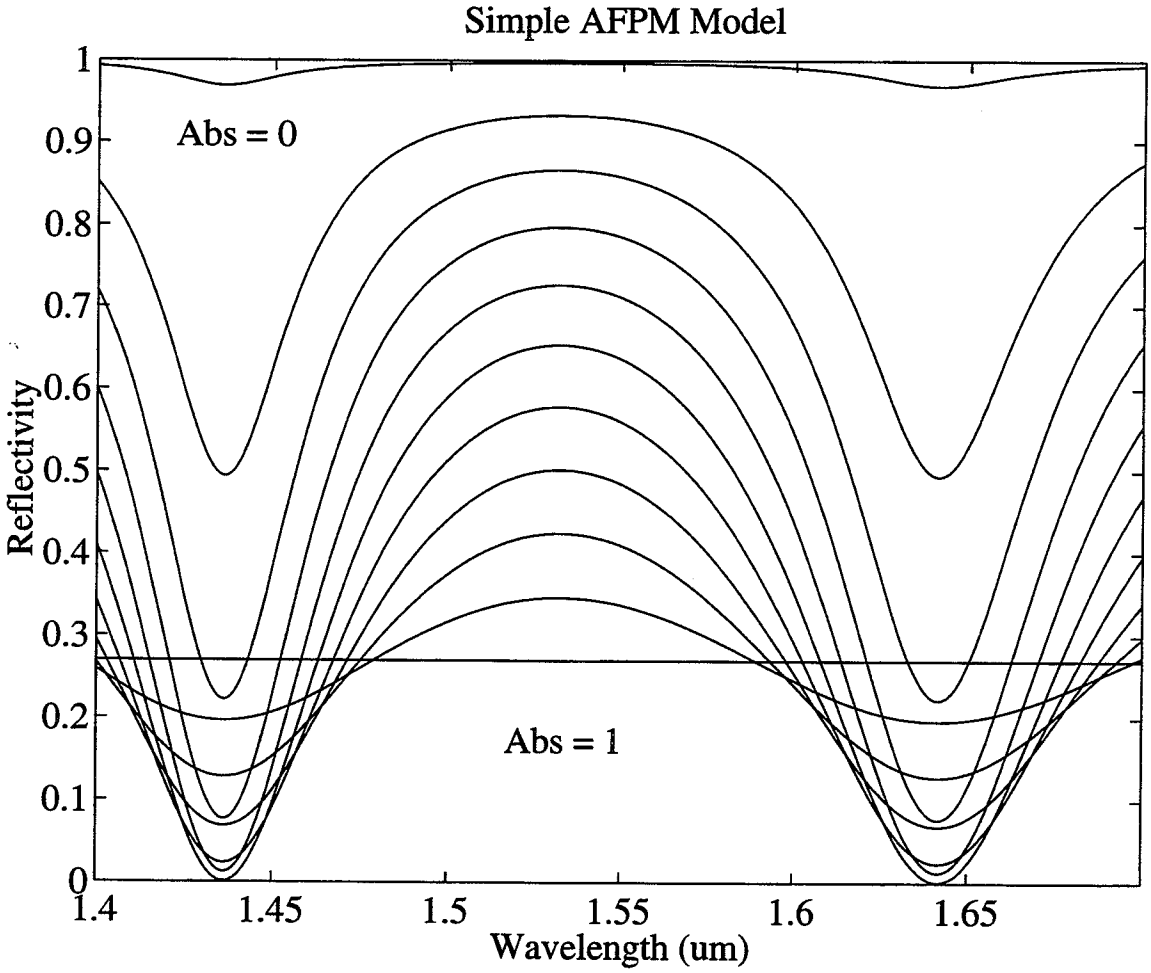


Fig. 4.5. Simple model calculation.

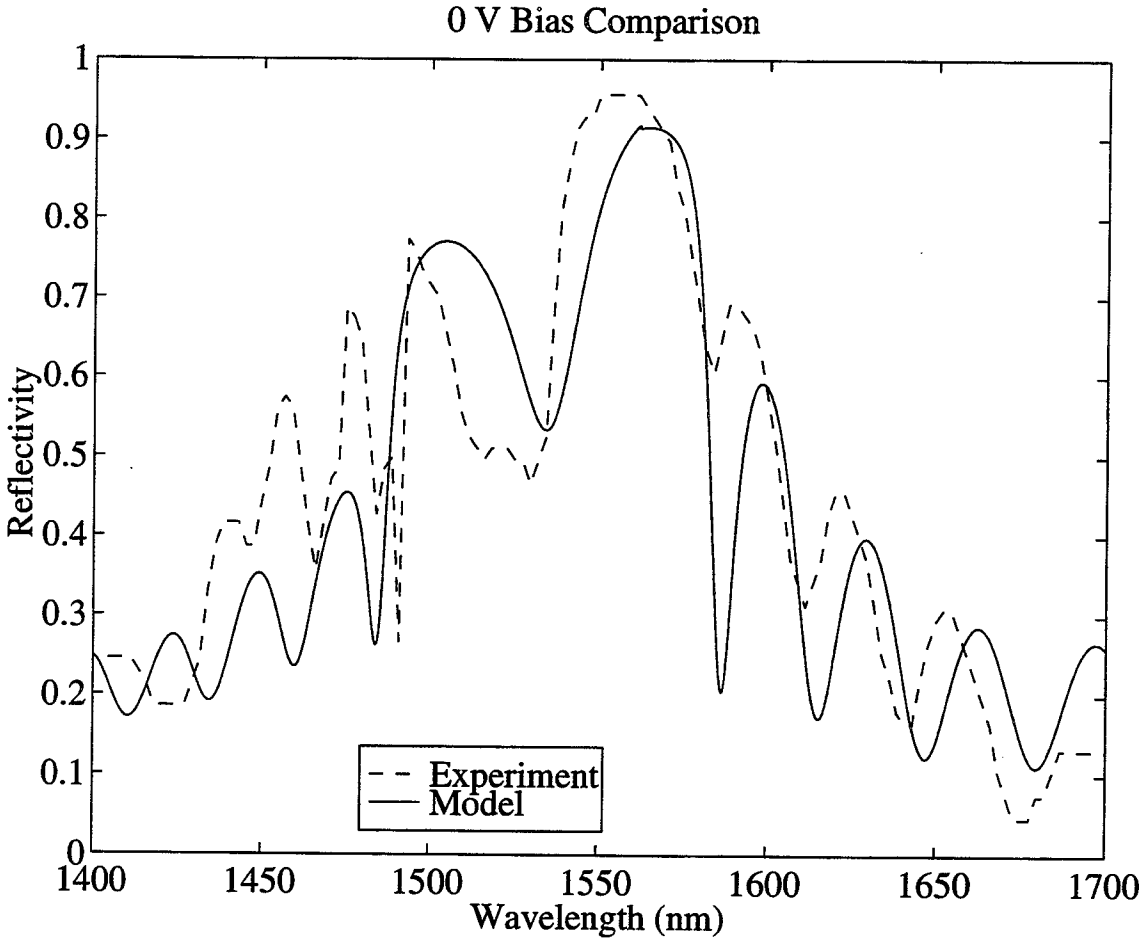


Fig. 4.6. Comparison between model and published measurements at 0V bias.

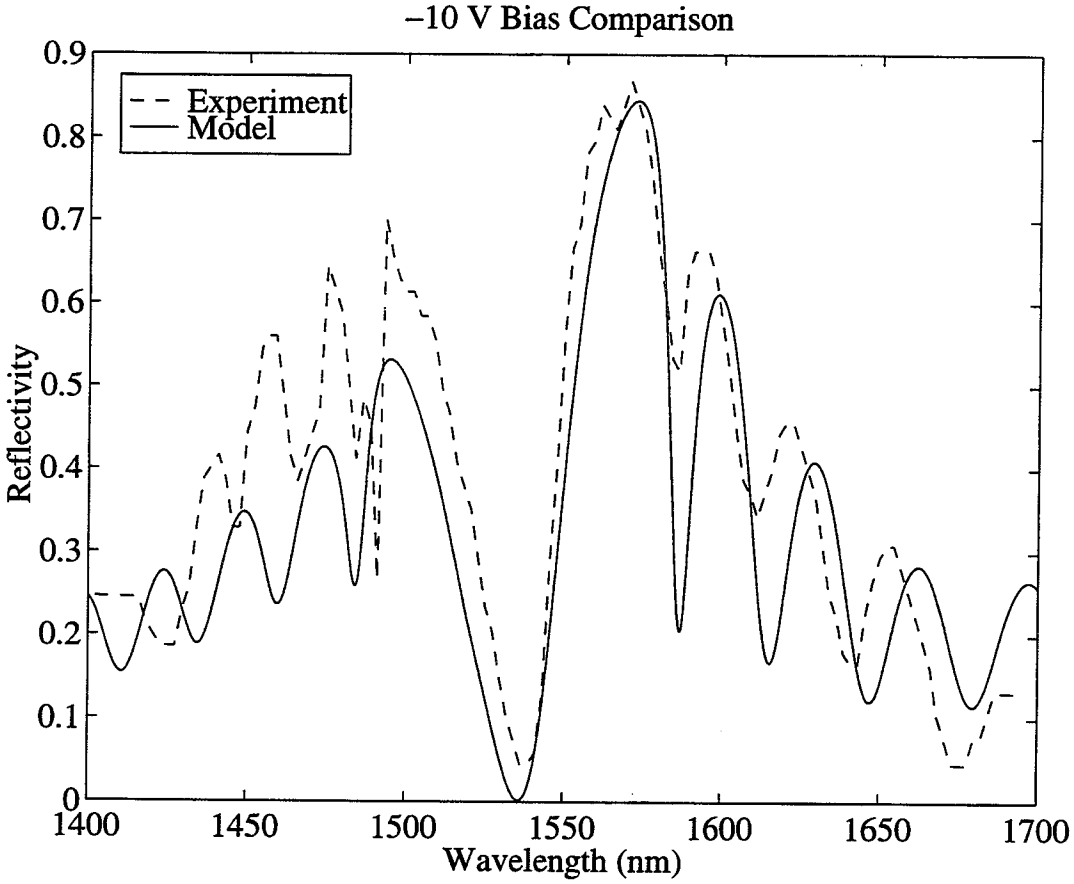


Fig. 4.7. Comparison between model and published measurements at -10V bias.

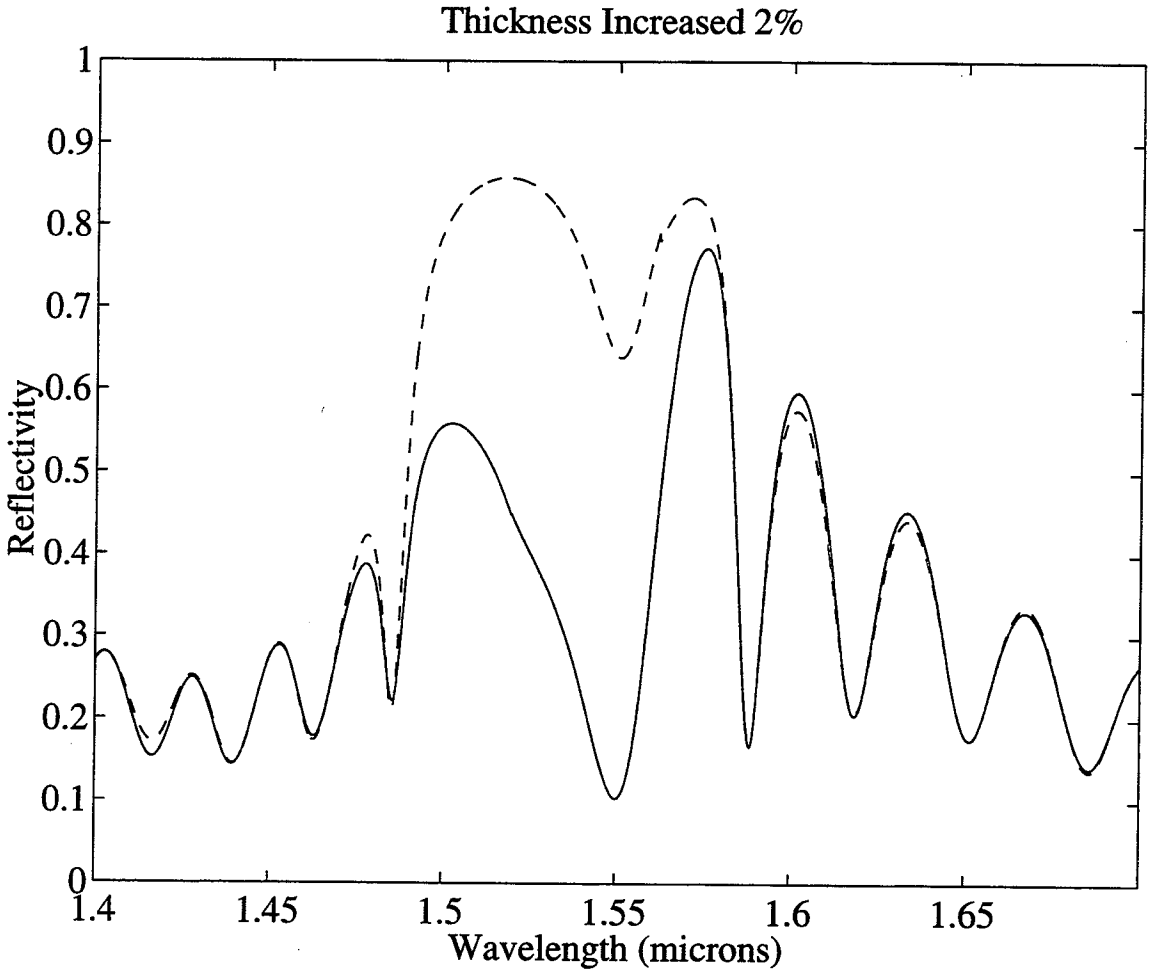


Fig. 4.8. Modeled reflectivity with cavity length increased by 2% for 0V bias (dashed) and -10V bias (solid).

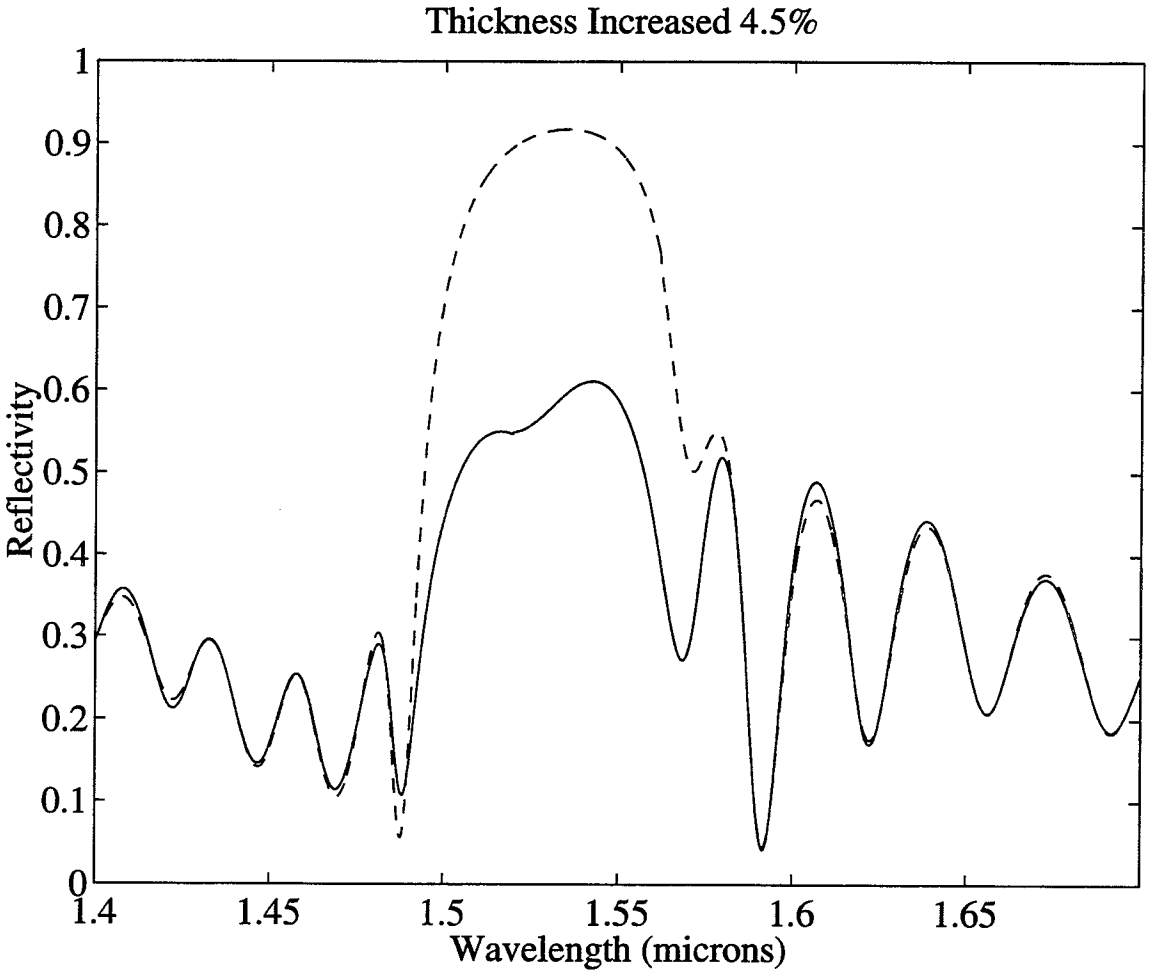


Fig. 4.9. Modeled reflectivity with cavity length increased 4.5% for 0V bias (dashed) and -10V bias (solid).

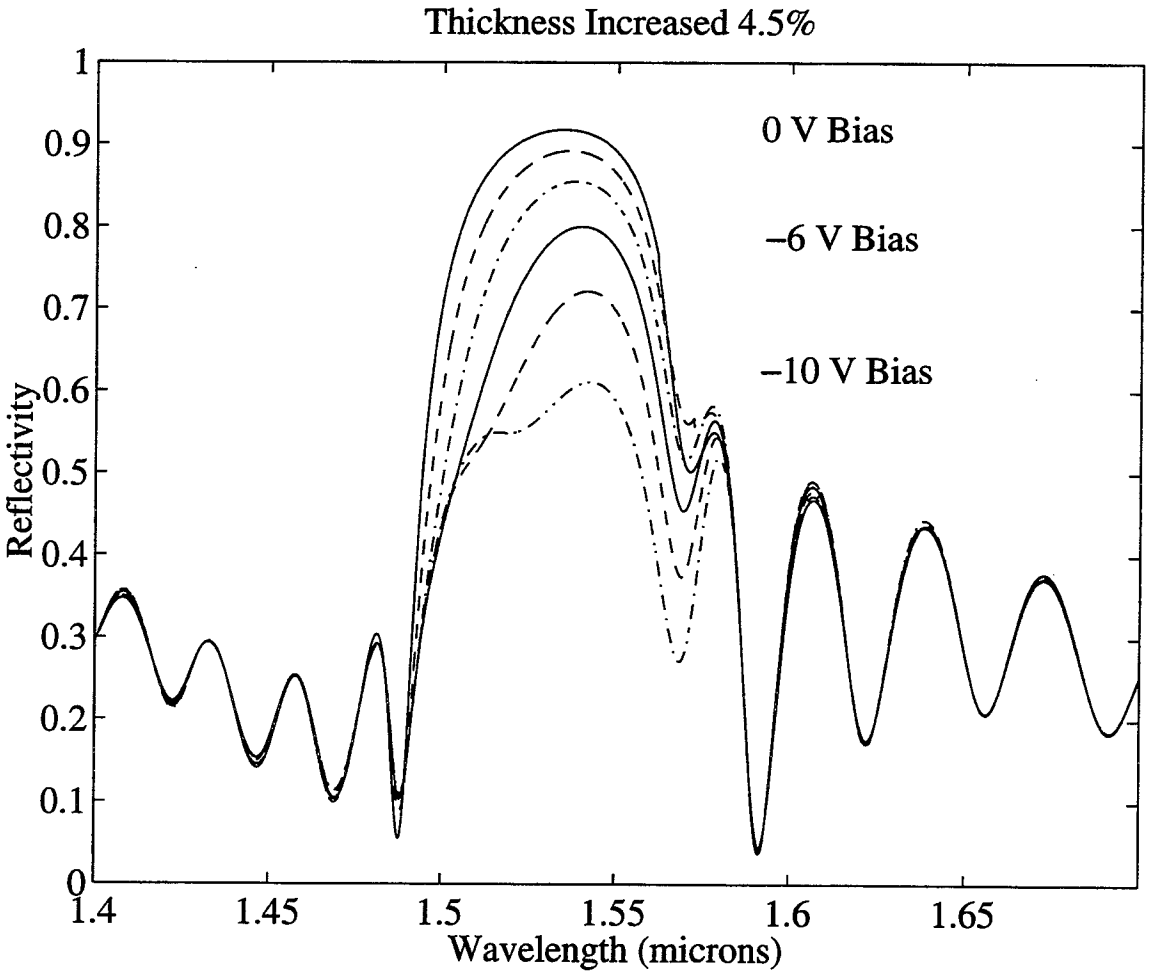


Fig. 4.10. Calculated reflectivity for a range of reverse bias conditions. Peak reflectivity decreases for increasing magnitude of electrical bias.

# 5. CONCLUSIONS & FUTURE WORK

In summary, the work presented here has demonstrated the design and construction of a moderate output power CW erbium fiber laser and DC characterization apparatus for use in performing reflectivity measurements on asymmetric Fabry-Perot reflection modulators in the 1.55 μm communications band. The devices tested to date show a radically decreased on-off contrast ratio compared to previous published results. The reason for this decreased contrast is explained by an error in the cavity length of the AFPM that modifies the resonance wavelength of the device in such a way that high on-off contrast is not possible to obtain with desirable low voltage biases.

Future experiments on devices such as these are certainly of interest. The characterization system has been constructed and proven to produce repeatable results. At such time as other device samples become available, the DC reflectivity can easily be measured using the techniques discussed herein.

# 6. REFERENCES

[1] A.M. Weiner, J.P. Heritage, and E.M. Kirschner, "High resolution coding of femtosecond pulses," *J. Opt. Soc. Amer.*, Vol. B5, pp. 1563, 1988.

[2] A.M. Weiner, D.E. Leaird, J.S. Patel, and J.R. Wullert, II, "Programmable shaping of femtosecond optical pulses by use of 128-element liquid crystal phase modulator," *IEEE J. Q. E.*, Vol. 28, No. 4, pp. 908-920, Apr. 1992.

[3] M.W. Maeda, J.S. Patel, D.A. Smith, Chinlon Lin, M.A. Saifi, and A. Von Lehman, "An electronically tunable fiber laser with a liquid-crystal etalon filter as the wavelength-tuning element," *IEEE Photonics Tech. Lett.*, Vol. 2, No. 11, pp. 787-789, Nov. 1990.

[4] P.F. Wysocki, M.J.F. Digonnet, and B.Y. Kim, "Electronically tunable, 1.55-μm erbium-doped fiber laser," *Opt. Lett.*, Vol. 15, No. 5, pp. 273-275, Mar. 1, 1990.

[5] D.A. Smith, M.W. Maeda, J.J. Johnson, J.S. Patel, M.A. Saifi, and A. Von Lehman, "Acoustically tuned erbium-doped fiber ring laser," *Opt. Lett.*, Vol. 16, No. 6, pp. 387-389, Mar. 15, 1991.

[6] K. Doughty, D.E.L. Vaughan, K. Cameron, and D.M. Bird, "Novel Acoustically Tuned Fiber Laser," *Elect. Lett.*, Vol. 29, No. 1, pp. 24-25, Jan. 7, 1993.

[7] J.L. Zyskind, J.W. Sulhoff, D.J. Digiovanni, L.W. Stulz, H.M. Presby, A. Piccirilli, and P.E. Pramayon, "Electrically tunable diode-pumped erbium-doped fibers ring laser with fiber Fabry-Perot etalon," *Elect. Lett.*, Vol. 27, No. 21, pp. 1950-1951, Oct. 10, 1991.

[8] C.V. Poulsen, and M. Sejka, "Highly optimized tunable $Er^{3+}$-doped single longitudinal mode fiber ring laser, experiment and model," *IEEE Photonics Tech. Lett.*, Vol. 5, No. 6, pp. 646-648, Jun. 1993.

[9] C.Y. Chen, M.M. Choy, M.J. Andrejco, M.A. Saifi, and Chinlon Lin, "A widely tunable erbium-doped fiber laser pumped at 532 nm," *IEEE Photonics Tech. Lett.*, Vol. 2, No. 1, pp. 18-20, Jan. 1990.

[10]R. Wyatt, "High-power broadly tunable erbium-doped silica fiber laser," *Elect. Lett.*, Vol. 25, No. 28, pp. 1498-1499, Oct. 26, 1990.

[11]C.R. o Cochlain, and R.J. Mears, "Broadband tunable single frequency diode-pumped erbium doped fiber laser", *Elect. Lett.*, Vol. 28, No. 2, pp. 124-125, Jan. 16, 1992.

[12]L. Reekie, R.J. Mears, S.B. Poole, and D.N. Payne, "Tunable single-mode fiber lasers", *J. Lghtwav Tech.*, Vol. LT-4, No. 7, pp. 956-960, Jul. 1986.

[13]P.F. Wysocki, private conversation.

[14]S.J.B. Yoo, R. Baht, and C. Caneau, "High-performance 1.5 μm operation of asymmetric Fabry-Perot modulators," in *Conference on Lasers and Electro Optics*, pp. 301, 1994.

[15]S.J.B. Yoo, R. Baht, C. Caneau, M.A. Koza, and T.P. Lee, "High-speed 1.5 μm asymmetric Fabry-Perot modulators," presented at *Opt. Fiber Conf.*, 1995.

[16]S. Ramo, J.R. Whinnery, and T. Van Duzer, *Fields and Waves in Communication Electronics*, New York: John Wiley & Sons, 1994, pp. 278-290.

[17]*OSA Handbook of Optics*, vol. 2, M. Bass, Ed., New York: McGraw Hill, 1995, pp. 33.63.

[18]B. Broberg, and S. Lindgren, "Refractive index of $In_{1-x}Ga_xAs_yP_{1-y}$ layers and InP in the transparent region," *J. Appl. Phys.*, Vol. 55, No. 1, pp. 3376-3381, May 1, 1984.

[19]*Landolt Bornstein, New Series, Group III*, vol. 22A, K.H. Hellwege, Ed., New York: Springer-Verlag, 1979, pp. 142.

[20]T. Takagi, "Refractive index of $Ga_{1-x}In_xAs$ prepared by vapor-phase epitaxy," *Jap. J. Appl. Phys.*, Vol. 18, No. 10, pp. 1813-1817, Oct. 1978.

[21]*Landolt Bornstein, New Series, Group III*, vol 22a, K.H. Hellwege, Ed., New York: Springer-Verlag, 1979, pp. 156.

[22]H. Dejun, and K.T. Chan, "Refractive index of AlInGaAs layers in the transparent wavelength region," in *IEEE Lasers and Electro-Optics Society 1994 7th Annual Meeting*, Vol. 2, 1994, pp. 349-350.

[23]D.K. Schroder, *Semiconductor Material and Device Characterization*, New York: John Wiley & Sons, 1990, pp. 468.

[24]T.Y. Chang, N.J. Sauer, and Y. He, "Optimization of molecular beam epitaxy grown pin multiple quantum well electroabsorption modulators for the 1.5-μm wavelength region," *J. Vac. Sci. Tech. B*, Vol. 11, No. 3, pp. 929-931, May 1993.

[25]A.K. Tipping, G. Parry, and A.J. Moseley, "Modeling the optimum performance of InGaAs/InP-based asymmetric Fabry-Perot modulator devices," *Semi. Sci. Tech.*, Vol. 5, pp. 525-529, 1990.

[26]C.J. Chang-Hasnain, J.P. Harbison, C. Zah, M.W. Maeda, L.T. Florez, N.G. Stoffel, T. Lee, "Multiple wavelength tunable surface-emitting laser arrays," *IEEE J. Q. E.*, Vol. 27, No. 6, pp. 1368-1376, Jun. 1990.